HEALTH AND MEDICINE

# Adipose-derived leptin and complement factor D mediate osteoarthritis severity and pain

**Kelsey H. Collins[1,2,3,4,5]*, Kristin L. Lenz[1,2,3], Hope D. Welhaven[5,6], Erica Ely[1,2,3,7], Luke E. Springer[8], Sophie Paradi[1,2,3,7], Ruhang Tang[1,2,3], Lauryn Braxton[1,2,3,7], Antonina Akk[8], Huimin Yan[8], Bo Zhang[3], Xiaobo Wu[8], John P. Atkinson[8], Arin K. Oestreich[1,2,3], Ron K. June[9], Christine T. N. Pham[8], Farshid Guilak[1,2,3,7]***



**Obesity is a risk factor for osteoarthritis (OA), and leptin is among the adipokines implicated in obesity-induced OA. However, the specific role of leptin in OA severity and pain is not known. Using lipodystrophic (LD) mice, we show that fat-secreted factors are required for knee OA development, implicating a fat-cartilage cross-talk. Fat pad implantation or systemic leptin restoration in LD mice reintroduced structural OA and pain, whereas implantation of leptin-deficient fat pad did not change OA susceptibility. Isochronic parabiosis and spatial transcriptomics confirmed that a fat-joint cross-talk likely occurred via soluble mediators. Global unsupervised multiomics of conditioned media from fat implants revealed that leptin exerts a regulatory effect on adipsin (or complement factor D), the activity of which modulates the contrastive OA structural and pain phenotype. These findings suggest that adipokines influence OA pathogenesis, providing conclusive evidence of a fat-joint cross-talk and implicating OA as a systemic disease of adipose tissue.**

## INTRODUCTION

Osteoarthritis (OA), a joint disease characterized by the progressive loss of cartilage lining articular joints, is a leading cause of pain and disability worldwide. Historically, OA has been dismissed as an inevitable disease of cartilage wear and tear that occurs with aging (*1*, *2*). This notion has hindered investigation into the underlying pathology and the development of disease-modifying drugs that slow or reverse joint degeneration. Current treatments rely mainly on pain management strategies, which are inadequate (*3*). As the aging population expands, there is an urgent need to delineate the pathological OA mechanisms to develop new therapeutic approaches that can modify joint structural changes and alleviate associated pain (*4*).

Previous studies have often focused on evaluating single tissues, such as cartilage and/or bone (*2*). However, an articular joint is a complex organ that can be affected by metabolic abnormalities found in a range of chronic conditions afflicting most patients with OA (59 to 87%) (*5*). For example, the population of patients with OA disproportionally consists of individuals who are obese and have abnormal metabolism (*6*). Although mechanical joint overloading has been proposed as an explanation for the relationship between obesity and OA, increased joint loading because of high body mass alone does not explain the spectrum of OA joint pathology (*7*, *8*).

While reducing body fat can alleviate some pain and mitigate OA progression (*9*), cartilage damage and pain persist even after weight loss. Although adipose tissue has long been considered inert, recent studies demonstrate a systemic influence through adipocyte endocrine function and resident immune cell populations (*10*). To investigate the contribution of fat to OA pathogenesis, we used a previously developed unique murine model, the lipodystrophic (LD) mouse that completely lacks typical visceral, subcutaneous, and brown adipose depots except for compensatory storage of lipids in the liver and muscle (*8*, *11*, *12*). We found that LD mice are protected from OA damage and pain (*8*), an effect reversed by exogenous extraarticular, subcutaneous fat pad implantation. A subsequent independent study has corroborated a causal role for systemic adipose tissue, rather than intraarticular adipose tissue, in OA pathogenesis (*13*). How extraarticular, implanted adipose tissue influences OA pathogenesis remains to be determined.

Leptin, a satiety hormone, is the most consistently increased fat-derived factor reported in obesity-induced OA (*14*, *15*). Unexpectedly, leptin knockout (KO) mice are protected from age-related OA despite being morbidly obese (*7*, *16*). However, the precise mechanistic role for leptin, its target tissue(s), and downstream mediators in OA is unknown. Leptin receptors are found on chondrocytes (*7*), osteoblasts (*17*), osteocytes (*17*), synoviocytes (*18*), bone marrow stromal cells (*19*), fat cells (*20*) in the knee joint, and sensory nerves (*21*) innervating the joint, suggesting that joint cells or tissues other than chondrocytes are also likely to transmit OA-inducing signals. Adding further complexity, previous work demonstrated that leptin alone was not sufficient to induce cartilage loss in osteochondral explants (*7*).

It is well established that the complement system plays a role in OA pathogenesis (*22*–*24*). The complement system is a critical component of innate immunity and wound healing (*25*), and loss-of-function mutations of several complement proteins result in protection from structural posttraumatic OA in mice (*24*). Complement activation can be initiated by antigen-antibody complexes through the classical pathway, carbohydrate moieties through the lectin pathway, or the alternative pathway that is activated when complement C3 is cleaved by the alternative pathway convertase C3bBb, generated by complement factor D (FD) mediated cleavage

[1]Department of Orthopaedic Surgery, Washington University in St. Louis, St. Louis, MO 63110, USA. [2]Shriners Hospitals for Children-St. Louis, St. Louis, MO 63110, USA. [3]Center of Regenerative Medicine, Washington University in St. Louis, St. Louis, MO 63110, USA. [4]Department of Orthopaedic Surgery, University of California, San Francisco, San Francisco, CA 94143, USA. [5]Department of Anatomy, University of California, San Francisco, San Francisco, CA 94143, USA. [6]Department of Chemistry & Biochemistry and Molecular Biosciences Program, Montana State University, Bozeman, MT 59717, USA. [7]Department of Biomedical Engineering, Washington University in St. Louis, St. Louis, MO 63105 USA. [8]Division of Rheumatology, Washington University in St. Louis, St. Louis, MO 63110, USA. [9]Department of Mechanical & Industrial Engineering, Montana State University, Bozeman, MT 59717, USA.
*Corresponding author. Email: kelsey.collins@ucsf.edu (K.H.C.); guilak@wustl.edu (F.G.)

of C3bB into C3bBb. FD, also known as adipsin, is a serine protease derived from adipose tissue (*26*). Complement activation is associated with cartilage damage, as shown by protection from the induction of posttraumatic OA using destabilization of the medial meniscus (DMM) in FD KO mice. However, previous investigations did not interrogate the direct role of FD in OA pain and behavior in the absence of FD (*22*, *27*, *28*). Our goal was to precisely and specifically target this mechanism to understand the mechanistic link between adipose tissue and pain in the knee joint. While previous studies have demonstrated associations between FD and leptin individually with OA (*23*), the two factors have not been considered together to understand their potential combinatorial, co-regulated, or downstream relationships that contribute to OA and pain. Here, we uncover a link between leptin and FD that motivated us to probe this potential causal relationship between fat and the onset of OA and pain.

In this study, we show that the leptin signal from fat affects the onset of both OA structural damage and pain. Furthermore, we perform experiments to understand how the leptin signal may be transduced from fat via soluble mediators to the joint using parabiosis and spatial transcriptomics. We also demonstrate that leptin may exert a regulatory effect on the expression of FD. We establish that FD cross-talk from fat with the joint modulates the OA pain phenotype. Collectively, this study provides conclusive evidence that leptin and FD play key roles in fat-joint cross-talk, resulting in structural OA and pain. More specifically, we establish that OA and musculoskeletal pain can result from systemic signals released from extraarticular adipose tissue.

## RESULTS

### Engineered systemic leptin KO fat protects against OA in LD mice

To restore adipose-derived leptin in a controlled manner in LD mice (which lack adipokines), we implanted either a wild-type mouse embryonic fibroblast–derived adipose (MEF-WT) implant, leptin KO MEF (MEF-KO) implant, or leptin heterozygous fat (MEF-HET) implant at 5 to 8 weeks of age (Fig. 1A) (*8*, *12*, *29*). We confirmed that leptin was significantly increased in MEF-WT and MEF-HET mice compared to LD and MEF-KO mice (Fig. 1B). Of note, the MEF-KO adipose implants grew to more than twice the size of MEF-WT and MEF-HET implants (Fig. 1C). LD mice implanted with MEF-WT had lower body mass than LD mice with MEF-HET and MEF KO implants (Fig. 1D) and lower body mass compared to LD mice with no implant. LD mice with MEF-KO implants lacking leptin had no liver mass changes compared to LD mice with no implant, while MEF-HET implants partially corrected the increased liver mass and MEF-WT implantation completely corrected the increased liver mass. LD mice with MEF-KO implants had an increased body fat percentage compared to WT and unmanipulated LD mice (Fig. 1E). These results demonstrate that MEF-WT implantation corrected the increased liver mass in LD mice.

We then wished to understand how fat implants with no leptin or one or two copies of the leptin gene affected joint structure and function. As previously observed (*8*), LD mice with MEF-WT implants challenged with OA-inducing DMM injury had similar joint structural damage to WT DMM mice, as assessed by the modified Mankin histology score (Fig. 1F). LD mice with MEF-HET implants had similar histology to LD mice with MEF-WT implants, suggesting that one copy of leptin is sufficient to reintroduce DMM-induced joint damage. Moreover, LD mice implanted with MEF-KO were protected from more severe DMM-induced damage, with similar modified Mankin scores to LD mice without an implant. Synovitis increased in DMM limbs from MEF-HET–implanted LD mice compared to nonsurgical controls, but there was no difference between MEF-HET and MEF-KO implantation (Fig. 1G). This disconnect between the synovitis phenotype and cartilage changes is consistent with that previously reported in LD mice (*8*). Osteophyte scores, a measure of bone formation in the joint, were higher in MEF-KO DMM limbs compared to nonsurgical limbs, while no differences were observed between MEF-HET DMM limbs and nonsurgical limbs (Fig. 1G). MEF implantation did not mitigate DMM-induced bone sclerosis in the medial tibia or medial femur, as measured by the bone volume fraction (BV/TV), but did reduce the bone mineral density (BMD) in both compartments (fig. S1). Concordantly, pressure-pain thresholds for hyperalgesia and mechanical allodynia were similar in LD mice and MEF-KO–implanted LD mice but were higher in the DMM limbs of LD mice implanted with MEF-WT and MEF-HET MEF (Fig. 1, H and I). Together, these results demonstrate that LD mice implanted with MEF-KO remained protected against cartilage damage and the onset of pain but not osteophyte formation.

Because LD mice have elevated levels of circulating inflammatory mediators and an insulin resistance phenotype compared to WT controls (*8*, *12*), we measured fasting insulin and glucose tolerance and systemic inflammatory profiles of the MEF-implanted mice. Relative to WT, all LD mice had reduced insulin tolerance as measured by the area under the curve (Fig. 1J), suggesting that the reversal of cartilage protection is independent of insulin sensitivity changes. We did not observe changes in glucose tolerance (Fig. 1K). Previous work demonstrated even low leptin levels were sufficient to reconstitute leptin signaling and induce damage (*8*). To understand the potential consequence of restoring leptin on the systemic inflammatory milieu, we profiled the serum from these mice using a multiplexed assay. Relative to WT mice, all MEF-implanted groups had similarly increased serum interleukin-1α (IL-1α) as was found in unmanipulated LD mice (Fig. 1L). LD mice implanted with MEF-WT had more circulating IL-6 compared to all groups (Fig. 1M). LD mice with MEF-KO implants had less circulating IL-10, nearing WT levels (Fig. 1N). Serum IL-17a in MEF-HET–implanted LD mice was significantly higher than that in WT and MEF-KO–implanted mice (Fig. 1O). LD mice implanted with MEF-WT demonstrated a trend toward more circulating monocyte chemoattractant protein–1 (MCP-1) compared to all groups (Fig. 1P), while all MEF-implanted groups had less circulating tumor necrosis factor–α (TNF-α) than LD mice (Fig. 1Q). Together, these data show that while MEF-WT and MEF-HET implantation reintroduced structural damage in the knee joint and corrected the increased liver mass to different degrees, the only significant change in systemic inflammatory mediators from the LD milieu was a decrease in TNF-α.

To understand whether MEF implantation altered the local knee joint environment, we profiled synovial fluid (SF) in these animals using a Luminex multiplex cytokine assay. Compared to the nonsurgical limb, IL-1α in SF from the DMM limb showed a trend toward a higher level in WT but was reduced in unmanipulated LD mice, while there were no changes in MEF-implanted LD mice (Fig. 1R). IL-6 and IL-10 were also lower in SF from the DMM limb of LD mice than in the nonsurgical limb, with no other changes observed

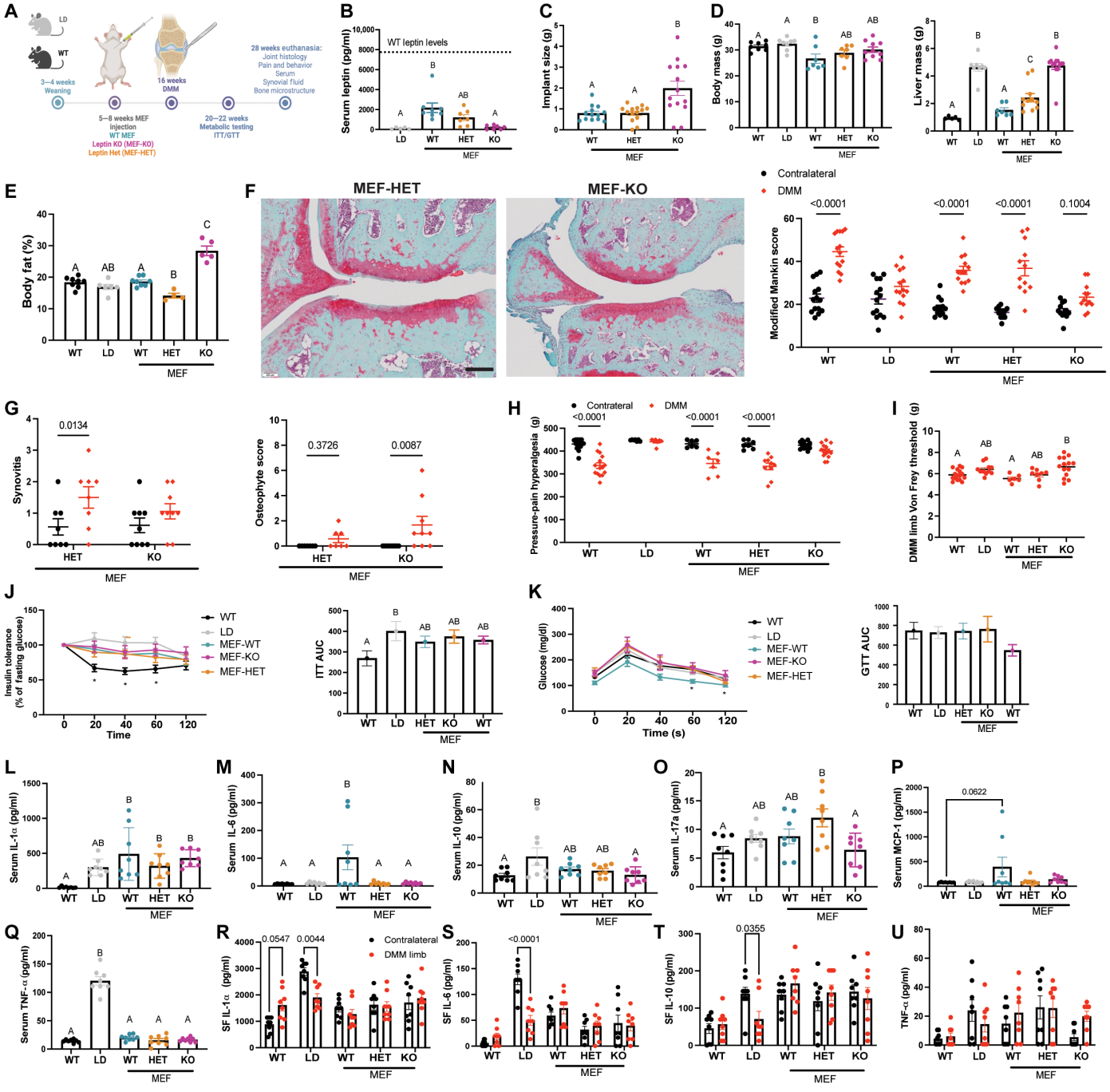


**Fig. 1. Adipose tissue is necessary for OA, but ablating fat–derived leptin protects knee joints from the onset of structural damage and pain.** (**A**) Experimental design and serum assessments for (**B**) leptin, (**C**) implant size, (**D**) body mass and liver mass, and (**E**) body fat. (**F**) Knee joint structural damage assessed by the modified Mankin score and medial tibial plateau images for Saf-O/Fast Green. The scale bar indicates 400 μm. (**G**) Synovitis score and osteophyte score. Pain measurements included (**H**) pressure-pain hyperalgesia at the knee and (**I**) Electronic Von Frey. (**J**) Insulin tolerance tests (ITT) and area under the curve (AUC) and (**K**) glucose tolerance tests (GTT) and area under the curve. Serum levels of (**L**) IL-1α, (**M**) IL-6, (**N**) IL-10, (**O**) IL-17a, (**P**) MCP-1, and (**Q**) TNF-α. SF levels for (**R**) IL-1α, (**S**) IL-6, (**T**) IL-10, and (**U**) TNF-α. $n = 4$ to 16 per group. Data were analyzed by one-, two-, or three-way ANOVA with Tukey, Sidak, or Bonferroni post hoc tests. Black, nonsurgical limb; red, DMM limb. Different letters indicate $P < 0.05$, or the exact $P$ value is shown for pairwise comparisons. Abbreviations: Ob/Ob, leptin KO mice; Ob/+, heterozygous mice; LD, LD mice; WT control mice; MEF-Ob, MEF with KO of leptin; MEF-Ob/+, MEF with het KO of leptin.

between limbs in any other groups (Fig. 1, S and T). Together, we found few differences in the local synovial inflammatory cytokine content of these animals when evaluated at 12 weeks post-DMM. Complete serum and SF profiles are listed in tables S1 and S2. These results may reflect the limitation and sensitivity of the multiplex assay in measuring SF cytokines in mice. Of note, sampling and profiling SF in mouse knee joints may not be representative of the inflammation in synovial joint tissues.

### Repletion of systemic leptin via an osmotic pump reverses OA and pain protection

To understand the impact of systemic leptin repletion in LD mice, and whether that would be sufficient to reintroduce cartilage damage and pain, we implanted LD mice with osmotic pumps 1 week before DMM to administer leptin (0.15 μl/hour) or saline over 6 weeks. To provide leptin throughout the 12-week follow-up post-DMM, the osmotic pump was replaced with a newly filled pump at week 5 post-DMM (Fig. 2A). Enzyme-linked immunosorbent assay (ELISA) results showed partial leptin level restoration in leptin-repleted mice compared to saline-treated and LD mice (Fig. 2B). Administration of leptin or saline did not change body mass. Compared to saline, leptin repletion significantly reduced the high liver mass previously reported in LD mice (*8*) but not to the WT level, likely due to partial repletion (Fig. 2, C and D).

Following DMM, cartilage damage increased compared to the nonsurgical limb in both saline- and leptin-administered LD mice. However, modified Mankin scores in saline-treated LD DMM limbs and untreated LD DMM limbs were significantly lower than those in WT DMM and leptin-repleted LD DMM limbs (Fig. 2, E and F). Both LD-treated groups demonstrated increased synovitis with DMM (Fig. 2G), but only saline-treated LD mice demonstrated an increase in osteophyte scores with DMM (Fig. 2H). No changes were observed in the bone microarchitecture assessments (BV/TV or BMD) by microcomputed tomography (microCT) in either saline- or leptin-treated LD mice compared to untreated LD mice (fig. S2). Only the leptin-repleted LD mice had reduced pressure-pain hyperalgesia and mechanical allodynia thresholds, comparable to WT DMM levels, but lower than untreated or saline-treated LD mice (Fig. 2, I and J). These results indicate that leptin repletion reversed the protection against the OA phenotype, synovitis, and pain in LD mice.

Group-specific differences in serum cytokine expression were identified (Fig. 2, K to P). Specifically, leptin repletion had the largest effect on reducing systemic TNF-α levels to similar levels observed in WT mice. Leptin did, however, increase circulating levels of IL-17a compared to WT. In the SF, there were no changes in the 18 factors measured in either leptin- or saline-treated LD mice with DMM (tables S3 and S4), except for reduced IL-1α, IL-4, IL-6, and IL-10 in DMM limbs of LD mice compared to nonsurgical contralateral LD limbs (Fig. 2, Q to U). Limitation in SF cytokine measurements, as noted above, restricts our ability to detect between-group differences.

### Fat-joint cross-talk is mediated via soluble factors

There are several plausible ways that fat may communicate with downstream joint issues. To provide insight on whether fat-derived secreted factors may be responsible for reversing the joint cartilage protection, we performed exploratory isochronic parabiosis, in which female LD mice were joined to female WT littermates at 5 to 8 weeks of age. Female mice were used in this experiment to avoid fighting behavior. At 16 weeks of age, DMM surgery was performed on the left limb of the LD (DMM-LD-L) mouse only (Fig. 3A) and compared to the nonsurgical right limb of the paired WT (WT-R) mouse. Because there were expected differences in joint loading because of the parabiotic pairings, we also evaluated the nonsurgical WT left (WT-L) limb and the nonsurgical LD right (LD-R) limb.

We first probed whether DMM injury would result in the chemotaxis of cells or cause the reconstitution of the infrapatellar fat pad. Following DMM challenge, immunohistochemical staining did not reveal any obvious reconstitution of the infrapatellar fat pad or infiltration of lipids in the DMM-LD-L mouse, with the space typically occupied by a fat pad filled with dense nonadipose tissue (Fig. 3B). We observed reductions in proteoglycan staining in the DMM-LD-L limbs, indicating a reversal of cartilage protection or joint damage ($n = 2$). As such, some of the cartilage regions of interest are missing in the spatial transcriptomic analysis (see below), as these limbs demonstrated cartilage damage from isochronic parabiosis by a WT pair (Fig. 3C).

Next, two isochronic parabiosis pairs were evaluated using 10x Visium spatial transcriptomics on formalin-fixed paraffin-embedded sagittal knee joint sections (Fig. 3C), which was a method we adapted to overcome the limitation of a lack of *Cre* drivers for the infrapatellar fat pad and synovium. As expected, no infiltrating adipose genes were identified in the infrapatellar region of the knee joint of DMM-LD-L limbs, indicating that the infrapatellar fat pad was not reconstituted in response to DMM injury. Therefore, we posit that factors secreted by fat are playing a role in OA pathogenesis.

This experiment allows for the quantification and identification of gene expression changes in the whole mouse joint with spatial resolution, which is a major advancement over typical methods that are restricted to a preselected probe set. We identified several tissue-specific populations of cells using graph-based comparisons and 8 to 12 clusters of spatially resolved cells (Fig. 3D). Unique molecular identifiers positive for the leptin gene *Lep* were located across the joint in multiple tissues (Fig. 3E). The leptin receptor *LepR* was located mostly in the bone marrow, consistent with a previous report (*11*) (Fig. 3F). In WT-R and WT-L limbs, adiponectin (*Adipoq*)–positive unique molecular identifiers colocalized in the infrapatellar fat pad, but no signal was observed in this corresponding area inferior to the fat pad in the LD mice (Fig. 3G).

In LD mice, the strongest *Adipoq* signal was in the tibial bone marrow, consistent with the notion that these mice do not reconstitute the infrapatellar fat pad in response to DMM injury or a shared blood supply with WT mice. In WT mice, we used *Adipoq* as a marker of the infrapatellar fat pad. We only identified one *Adipoq*-overlapping factor in these samples, FD in the infrapatellar fat pad region of WT mice (Fig. 3H). *Prg4*, a marker of synovium and superficial zone cartilage (*30*), was reduced in the DMM-LD-L limb compared to the LD-R limb, suggesting that isochronic parabiosis was sufficient to induce cartilage damage, as evidenced by reduced proteoglycan content (toluidine blue stain) observed in the DMM-LD-L limb (Fig. 3B).

We leveraged the internal LD-R and WT-L limbs to characterize changes in gene expression profiles of joint tissues using spatial transcriptomics. These limbs were partially unloaded because of the parabiosis procedure but were exposed to the same blood supply. In LD-R limbs, which were not challenged with DMM and were joined with the WT-L limbs, the top four differentially regulated genes

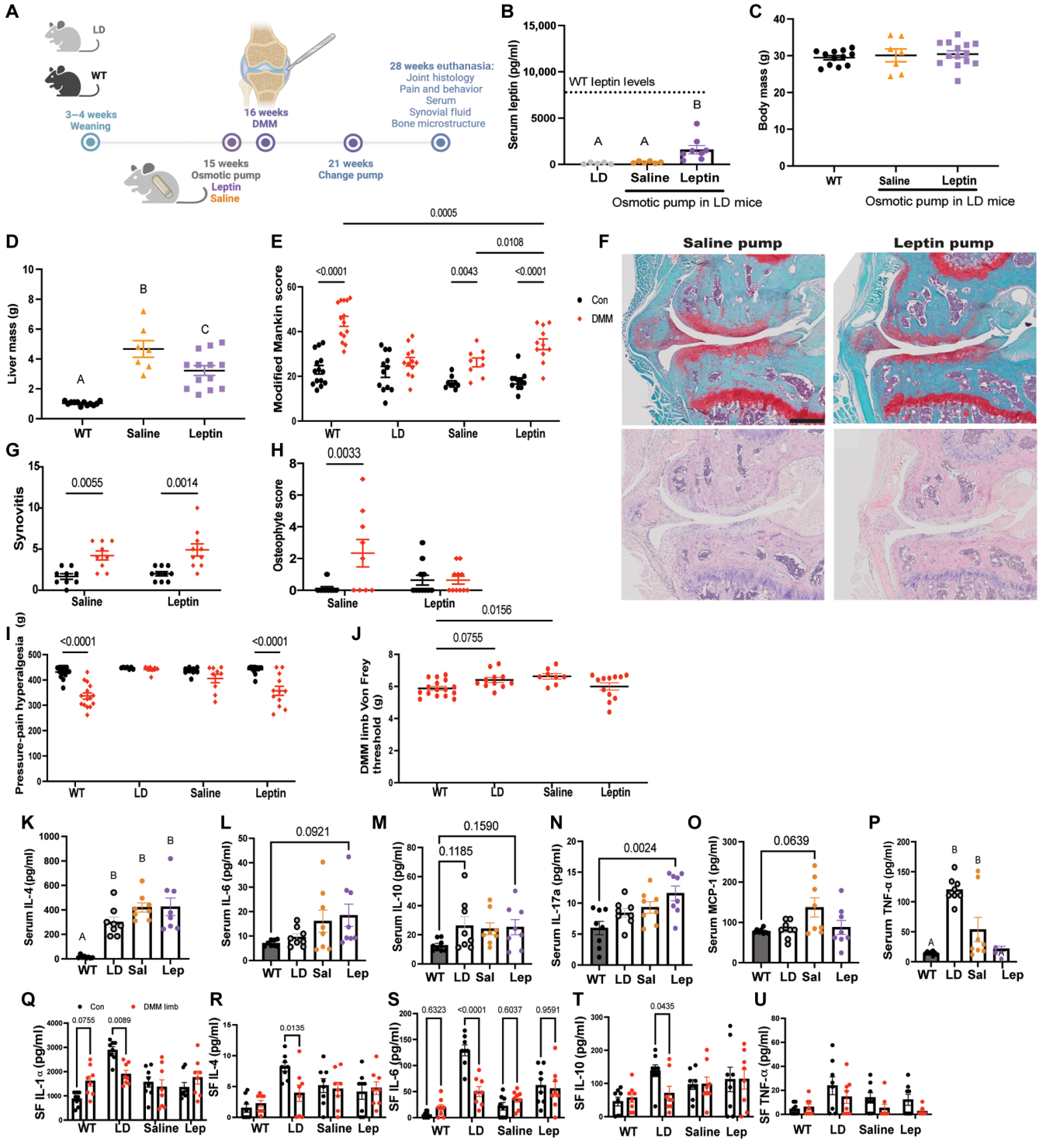


**Fig. 2. Reintroducing leptin systemically via an osmotic pump reverses cartilage protection in LD mice.** (**A**) Experimental design and serum assessments for (**B**) leptin and (**C**) body mass and (**D**) liver mass. (**E**) Knee joint structural damage assessed by the modified Mankin score and (**F**) medial tibial plateau images for Safranin-O/Fast Green and hematoxylin and eosin. The scale bar indicates 200 μm. Con, contralateral. (**G**) Synovitis score and (**H**) osteophyte score. Pain measurements included (**I**) pressure-pain hyperalgesia at the knee and (**J**) Electronic Von Frey. Serum measurements for (**K**) IL-4, (**L**) IL-6, (**M**) IL-10, (**N**) IL-17a, (**O**) MCP-1, and (**P**) TNF-α. SF levels for (**Q**) IL-1α, (**R**) IL-4, (**S**) IL-6, (**T**) IL-10, and (**U**) TNF-α. $n = 8$ to 14 per group. Data were analyzed by one-, two-, or three-way ANOVA with Tukey, Sidak, or Bonferroni post hoc tests. Black, nonsurgical limb; red, DMM limb. Different letters indicate $P < 0.05$, or the exact $P$ value is shown for pairwise comparisons. Abbreviations: LD, LD mice; Sal/Saline, saline osmotic pump in LD mouse; Lep, leptin osmotic pump in LD mouse; WT, control mice.

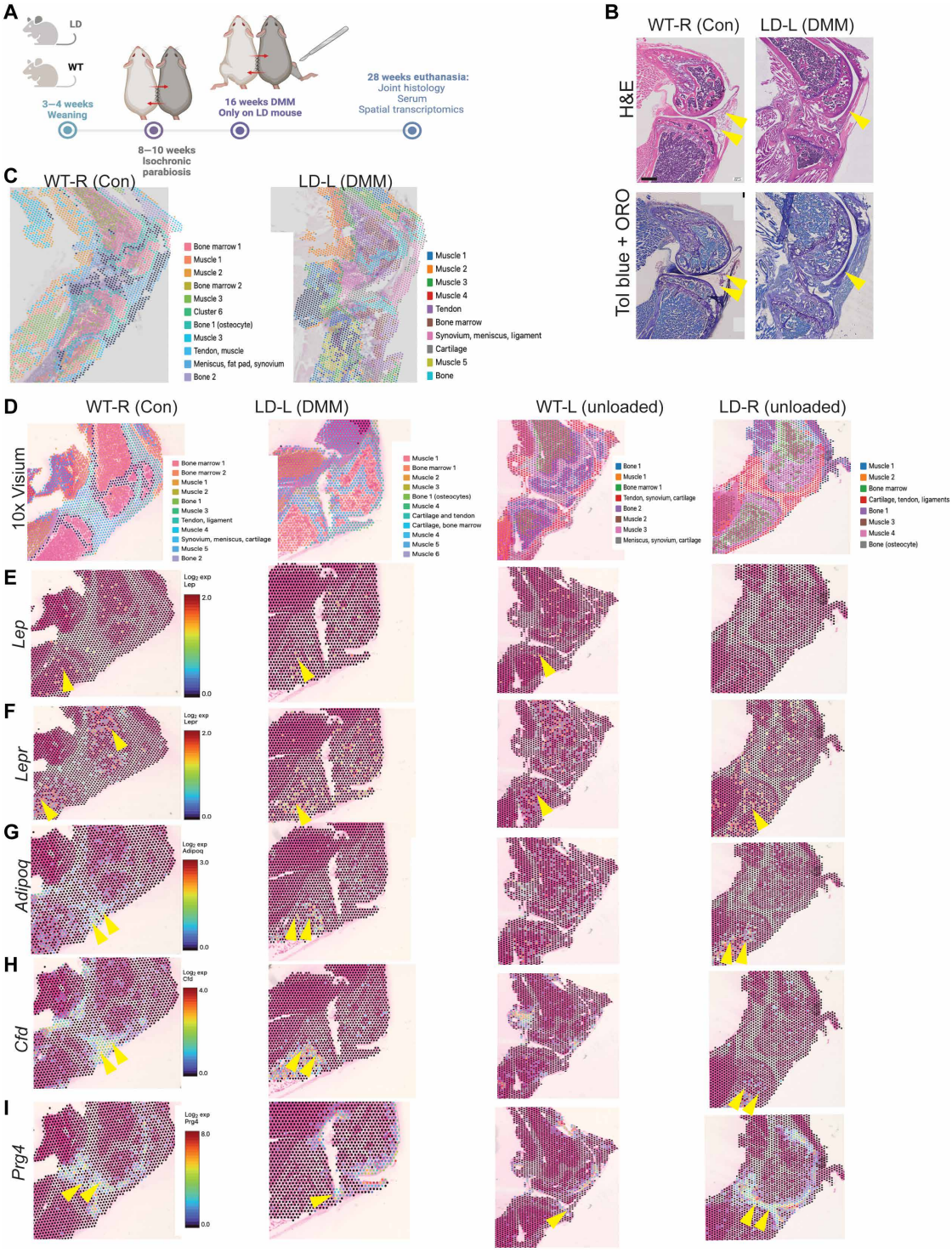


**Fig. 3. LD mice demonstrate cartilage damage when joined by isochronic parabiosis with DTA littermates but do not reconstitute the infrapatellar fat pad.** (**A**) Experimental design, (**B**) hematoxylin and eosin (H&E) and toluidine blue (Tol blue; proteoglycan) counterstaining with oil red O (ORO; lipid), (**C**) formalin-fixed, paraffin-embedded 10x Visium with CytAssist barcodes 12 weeks after DMM, (**D**) spatial barcoding for WT-R (nonsurgical), WT-L (nonloaded), LD-R (nonloaded), and LD-L (challenged with DMM), and spatial gene arrays for (**E**) leptin, (**F**) leptin receptor, (**G**) adiponectin, (**H**) FD, and (**I**) Prg-4.

(*Cfd*, *Prg4*, *Fasn*, and *Thrsp*) were observed in the synovium, meniscus, and cartilage clusters (Fig. 3, J and K). These four genes also defined the same clusters in the WT-L unloaded limb. The spatially analogous clusters in the DMM-LD-L limb were also the most differentially regulated, defined by *Prg4*, *Fn1*, and *Col3a1*. The most differentially regulated genes in the cartilage clusters in LD-L limbs were *Col2a1*, *Sost*, *Comp*, *Col9a1*, *Clec3a*, and *Chad*. Changes in these genes were also observed in the LD-R synovium and cartilage cluster. In DMM-LD-L joints evaluated, the FD (*Cfd*) signal localized to the tibial bone marrow, similar in location to adiponectin expression and indicating a change in the *Cfd* expression between LD and WT mice, because of an absence in the infrapatellar fat pad. In summary, we did not identify a specific tissue or cell type targeted by *Lep* or *LepR* but observed several genes differentially expressed with spatial resolution. Specifically, we identified that *Cfd* is localized to the infrapatellar fat pad in WT-R limbs, which may be related to vulnerability to DMM in WT mice.

## MEF implant transcriptomics reveals genes related to complement signaling

To determine whether DMM-induced joint damage can influence distal extraarticular adipose tissue (outside of the joint infrapatellar fat pad), bulk RNA was isolated from the visceral adipose tissue of WT male mice 16 weeks after DMM surgery and subjected to bulk RNA sequencing (RNA-seq). A total of 1523 genes was differentially regulated—782 up-regulated with DMM and 741 down-regulated with DMM—suggesting that unilateral cartilage injury and the OA phenotype in the joint can induce changes in distal visceral adipose tissue outside the knee joint (Fig. 4A). Kyoto Encyclopedia of Genes and Genomes (KEGG) pathway analysis revealed differential enrichment

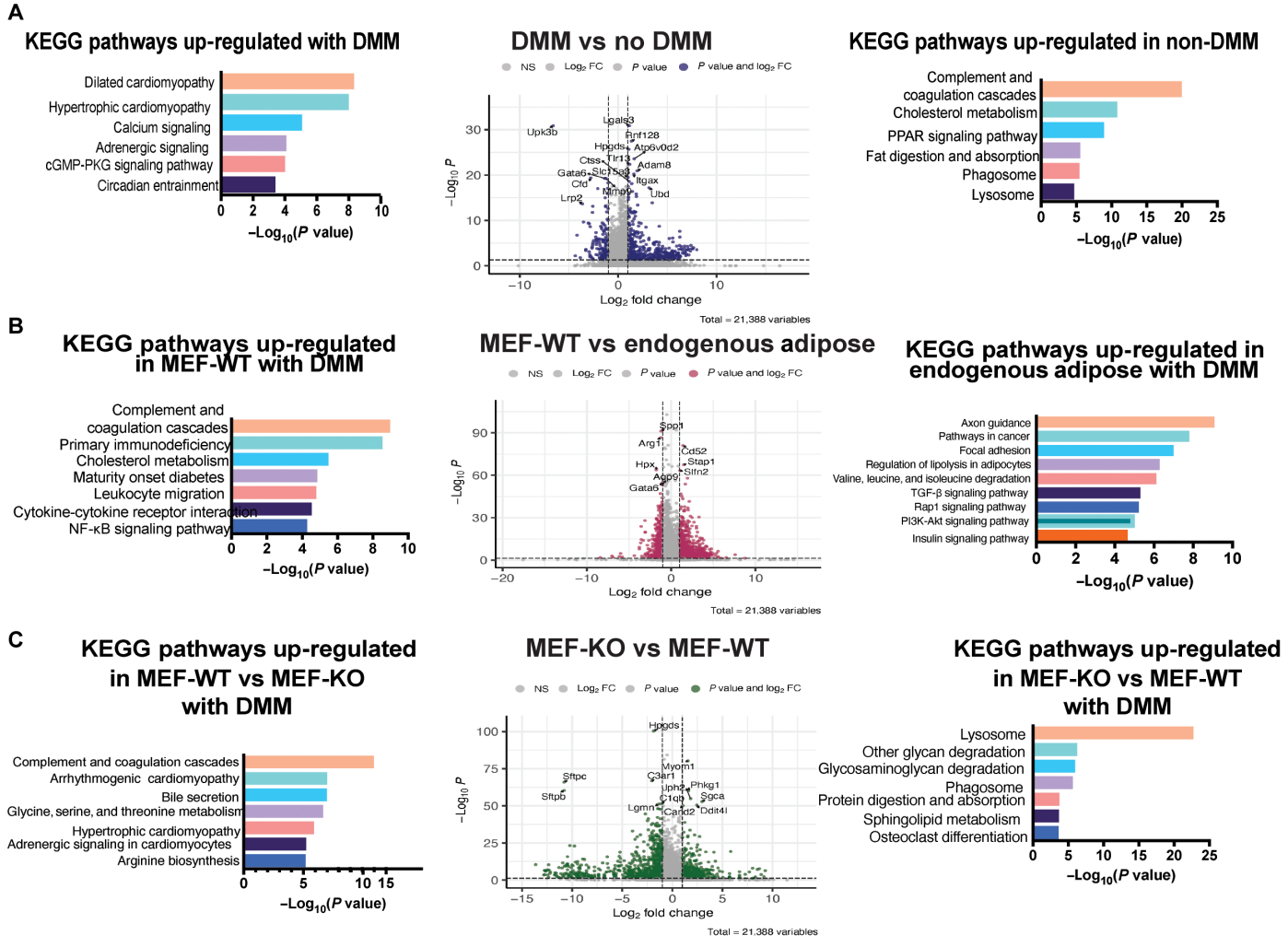


**Fig. 4. Joint damage induces changes to bulk transcriptomic profiles in adipose tissue, which are consistent with MEF implants and point to complement signaling in the reintroduction of OA.** (**A**) KEGG pathways up-regulated in adipose with DMM by adipose tissue bulk sequencing, violin plot for differential expression between adipose with (blue) and without DMM (orange), and KEGG pathways up-regulated in adipose without DMM. NS, not significant. (**B**) KEGG pathways up-regulated in WT implanted (MEF-WT) adipose with DMM compared to endogenous visceral adipose with DMM by adipose tissue bulk sequencing, violin plot for differential expression between MEF-WT adipose with DMM (blue) and endogenous visceral adipose with DMM (orange), and KEGG pathways up-regulated in endogenous visceral adipose with DMM. (**C**) KEGG pathways up-regulated in leptin KO (MEF-KO) adipose with DMM compared to MEF-WT adipose with DMM by adipose tissue bulk sequencing, violin plot for differential expression between MEF-KO with DMM (blue) and MEF-WT with DMM (orange), and KEGG pathways up-regulated in MEF-WT compared to MEF-KO.

in pathways associated with cardiomyopathy, calcium signaling, adrenergic signaling, and circadian entrainment (Fig. 4A). The most highly up-regulated pathways in adipose tissue of nonoperated limbs compared to adipose tissue of DMM mice included complement and coagulation pathway proteins, peroxisome proliferator–activated receptor γ (Pparγ) signaling pathway (the master regulator of adipogenesis), and pathways related to fat digestion and absorption (Fig. 4A).

While MEFs have been used in a variety of capacities to understand adipose signaling and metabolism, there is a paucity of information characterizing these tissues upon implantation. We previously demonstrated that in vivo MEF-WT implants secrete factors like subcutaneous adipose tissue (*12*), but the transcriptional changes have not been defined. In comparing the bulk transcriptome of MEF-WT implants to that of endogenous visceral adipose tissue following DMM surgery, the top differentially regulated pathways by KEGG were complement and coagulation cascades and pathways related to immunodeficiency in implanted MEF-WT (Fig. 4B). In endogenous adipose, axon guidance, focal adhesion, transforming growth factor–β signaling, Rap1 signaling, and phosphatidylinositol 3-kinase-AKT signaling pathways were among the most differentially regulated. Because MEF-KO mice were protected from DMM-induced OA, we compared MEF-WT to MEF-KO fat implants. In MEF-WT implants, KEGG analysis indicated that complement and coagulation cascade pathways were the most differentially regulated in the MEF-WT fat explants compared to MEF-KO (Fig. 4C), confirming the importance of these pathways in fat in response to DMM-induced OA. Together, these data suggest that either complement activity is influenced by leptin signaling or perhaps complement factors are co-regulated by the same factors as leptin.

### Multiomic profiling of the MEF implant secretome reveals a leptin-FD link

To identify factors secreted from fat that may play a causal role in conferring vulnerability to cartilage damage with DMM, we examined the MEF implant secretome following DMM in LD mice. Leveraging a new dual extraction protocol we developed, the metabolome and proteome were isolated from the same sample for global untargeted analysis by liquid chromatography–mass spectrometry. Specifically, generated conditioned media (CM) from MEF-WT, MEF-KO, and MEF-HET implants harvested at 16 weeks after DMM were collected and underwent a dual multiomic extraction.

We first evaluated the content of the samples. A total of 5194 metabolites was codetected across all samples. To distinguish populations of features that are differentially regulated between MEF-WT and MEF-KO CM, volcano plot analysis was performed and showed that 190 metabolites were higher in concentration in MEF-KO compared to MEF-WT, whereas 204 were higher in MEF-WT (Fig. 5A). Partial least-squares discriminant analysis (PLS-DA) showed a distinct separation between MEF-KO and MEF-HET from MEF-WT (Fig. 5B). Additional analyses including principal components analysis and analysis of variance (ANOVA) were performed to assess metabolic differences associated between MEF-WT, MEF-KO, and MEF-HET (fig. S4). Median intensity heatmap analysis was performed to visualize global differences across the metabolome of MEF-WT, MEF-KO, and MEF-HET to identify patterns or clusters of co-regulated and differentially expressed metabolites. Metabolite analysis revealed that factors related to glycosaminoglycan degradation were the highest in concentration in MEF-KO CM but lower in MEF-HET and MEF-WT CM (Fig. 5C, cluster 1). Conversely, metabolites involved in fatty acid metabolism and amino acid metabolism were the highest in concentration in MEF-WT CM compared to MEF-HET or MEF-KO CM (Fig. 5C, clusters 3 and 4). Additional pairwise comparisons were performed to further examine differences in metabolites between MEF-WT, MEF-KO, and MEF-HET (fig. S4).

In total, 22,861 peptides were identified, corresponding to 282 whole proteins. FD was differentially up-regulated in MEF-WT CM versus MET-HET CM and MEF-WT CM compared to MEF-KO (Fig. 5, D and E). FD is specifically secreted by adipose tissue (*26*) and has previously been mechanistically demonstrated to play a role in cartilage damage in OA (*22*, *28*, *31*, *32*). Other conserved differentially regulated factors include serpin a1e and neutrophilic granule protein, which are also implicated in OA pathogenesis, with unknown mechanisms of action. These results corroborate findings from spatial transcriptomics that, specifically, FD plays an important role in the fat-joint cross-talk.

Leptin is known to induce pro-inflammatory mediators, specifically in macrophages (*33*), but requires a combinatory activation of lipopolysaccharide (LPS; both at doses of 100 ng/ml) (*34*). This finding is concordant with previous work (*7*) that demonstrated that leptin alone is not sufficient to induce damage in chondrocytes. To understand the mechanistic role of leptin in the present context, in combination with low-level systemic inflammation, we isolated primary mouse bone marrow–derived macrophages (BMMϕ's), challenged them with LPS and leptin (100 ng/ml) (*33*, *34*), and measured the resulting inflammatory mediator production in media by a cytometric bead array assay (fig. S5). As expected, leptin alone did not increase a select subset of inflammatory markers measured. Moreover, LPS increased the levels of pro-inflammatory mediators, IL-1, IL-6, and TNF-α, as well as the anti-inflammatory mediator IL-10. Leptin + LPS significantly increased the levels of IL-1, IL-6, and TNF-α compared to LPS alone. Leptin alone did not increase these mediators. We then leveraged primary BMMϕ's from $FD^{-/-}$ mice and compared their response to LPS + leptin to WT BMMϕ's. We observed that primary $FD^{-/-}$ BMMϕ cells had a blunted response to LPS + leptin compared to WT BMMϕ cells. However, it is not clear what the cellular or tissue transducer of fat-secreted leptin is, and these data suggest that FD is partially required for the leptin response in primary BMMϕ cells.

### FD regulates OA structure and pain

To understand how FD contributes mechanistically to fat-joint cross-talk and induces initiation of the OA phenotype, we implanted global $FD^{-/-}$ mice with MEF-WT to restore circulating FD (Fig. 6A) (*26*). Consistent with previous reports, the loss of complement proteins and FD protected cartilage against OA-related damage (Fig. 6, B and C) (*22*, *23*, *28*). The protection was reversed to WT DMM levels in $FD^{-/-}$ animals implanted with MEF-WT (Fig. 6, B and C). Despite the cartilage protection, $FD^{-/-}$ mice had more synovitis and osteophytosis than WT and FD-KO + MEF-WT in the DMM limbs (Fig. 6, D to F). Unexpectedly, $FD^{-/-}$ mice, despite reduced modified Mankin scores, had heightened pressure-pain hyperalgesia, which was reversed in $FD^{-/-}$ mice implanted with MEF-WT (Fig. 6G). This pain phenotype was not explained by the synovitis scores (Fig. 6H) and appeared to be specific to hyperalgesia because allodynia, as measured by Electronic Von Frey, was not reduced (Fig. 6I). $FD^{-/-}$ mice also exhibited increased DMM-induced medial tibial subchondral bone thickening despite the lack of cartilage damage (fig. S6).

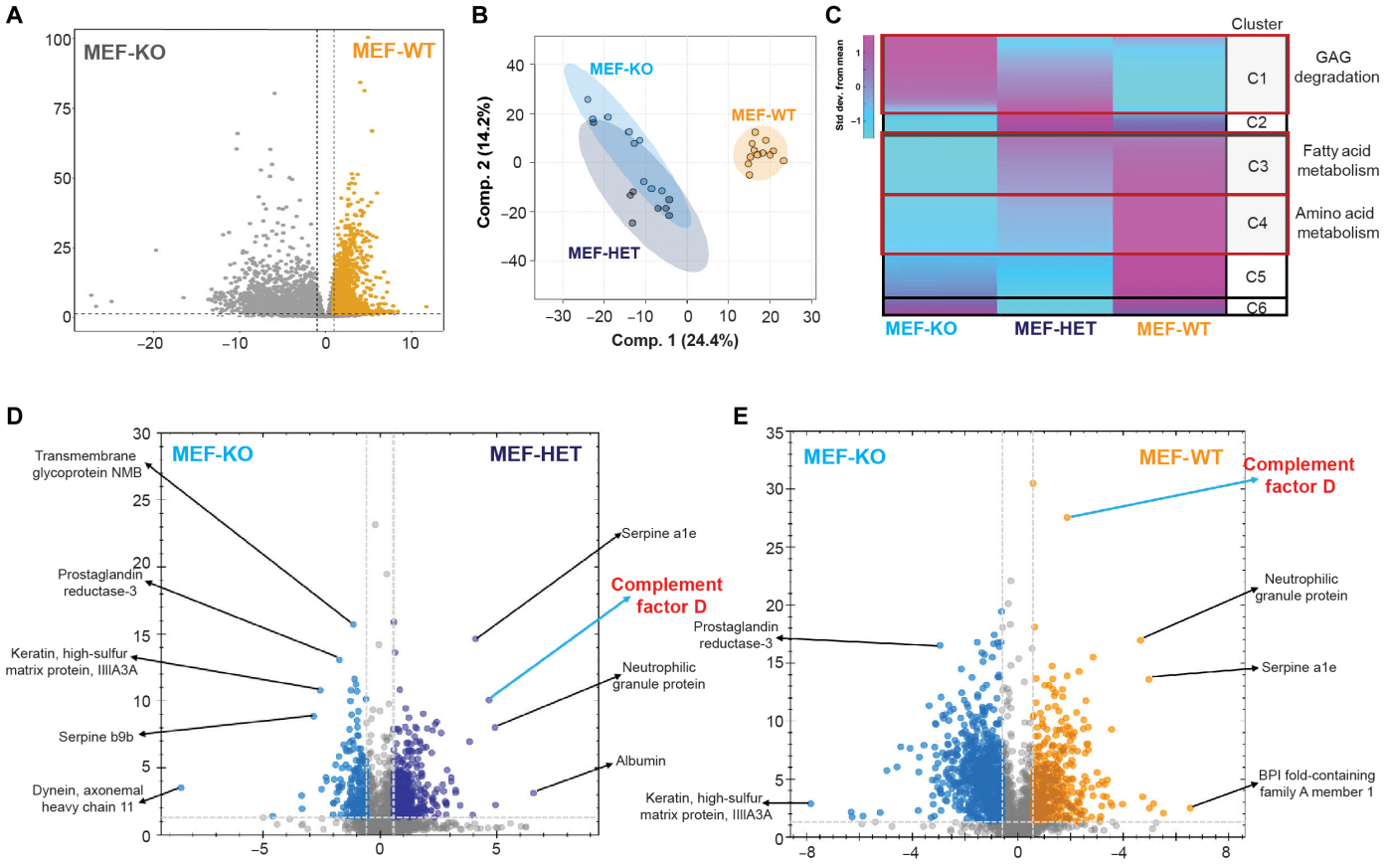


**Fig. 5. Untargeted metabolomic and proteomic analyses identify FD as a consistent differentially secreted protein by fat in the reversal of cartilage protection.** (**A**) Volcano plot identified 394 metabolites that differ between MEF-KO and MEF-WT (190 highest in MEF-KO and 204 highest in MEF-WT), (**B**) PLS-DA plot, (**C**) median intensity heatmap, and volcano plot of differentially expressed proteins between (**D**) MEF-KO and MEF-HET and (**E**) MEF-KO and MEF-WT.

To confirm that loss of FD did not change the global metabolic status of mice, we profiled their insulin and glucose tolerance. $FD^{-/-}$ mice demonstrated normal insulin tolerance and fasting glucose tolerance compared to WT and $FD^{-/-}$ + MEF-WT mice (Fig. 6, J and K), even though both $FD^{-/-}$ and $FD^{-/-}$ + MEF-WT mice had significantly reduced body fat compared to WT (Fig. 6L), suggesting that loss of FD does not result in a systemic metabolic change in mice. We observed increased marrow adipocytes in the tibiae of $FD^{-/-}$ with DMM compared to WT with DMM and $FD^{-/-}$ without DMM, which was reversed in $FD^{-/-}$ mice with MEF treatment (fig. S7).

To determine whether complement activation was detectable in the DMM joint, we performed immunohistochemistry on joint sections to examine for complement factors. As expected, we saw no complement activation in the DMM limb of $FD^{-/-}$ mice (fig. S8). Conversely, we found that the systemic milieu was altered in the $FD^{-/-}$ mice. For example, serum leptin was significantly lower in both $FD^{-/-}$ and $FD^{-/-}$ + MEF-WT mice (Fig. 6M), concordant with reduced body fat (Fig. 6L), while body weight was not different between groups (Fig. 6N). Moreover, both $FD^{-/-}$ and $FD^{-/-}$ + MEF-WT animals had more circulating IL-1α (Fig. 6O) but reduced IL-6 (Fig. 6P) and MCP-1 (Fig. 6R) in their serum. IL-10 and TNF-α were significantly lower in $FD^{-/-}$ + MEF-WT compared to WT, whereas both were partially reduced in $FD^{-/-}$ (Fig. 6, Q and S). Minor changes, including increased IL-6 and no change in IL-10, were detected in the SF of WT and $FD^{-/-}$ + MEF DMM limbs compared to WT limbs (Fig. 6, T and U).

Dorsal root ganglion (DRG) neurons are sensory neurons that transmit pain signals to the brain. To further our understanding of the knee pressure-pain hyperalgesia phenotype we uncovered in $FD^{-/-}$ mice, we performed bulk sequencing on L3-L5 DRGs, which provide sensory innervation to the knee joint, and compared sensory nerve gene transcription in $FD^{-/-}$ to WT mice. In WT mice, we observed enriched KEGG terms, including cardiac muscle contraction and adrenergic signaling, in the DMM limb compared to the contralateral limb (Fig. 7A). In $FD^{-/-}$ DRGs challenged with DMM compared to nonsurgical $FD^{-/-}$ DRGs, we only observed two significantly differentially regulated genes: TCHH (trichohyalin; which plays a role in keratinization and nervous system development/axon guidance and is involved in gene ontology terms that enable calcium ion binding) and GM29443 (which has an unknown role in the mouse genome). In the nonsurgical $FD^{-/-}$ DRGs, we observed differences in pathways associated with calcium signaling and cardiac muscle contraction. In WT DMM mice compared to $FD^{-/-}$, neutrophil extracellular trap formation, primary immune deficiency, and hematopoietic cell lineage were up-regulated. In $FD^{-/-}$ versus WT DRGs, the most prominent enriched KEGG terms were associated with cardiac muscle contraction, which was driven by expression of the following genes: TNNC1, TPM2, TPM1, CASQ2, HRC, ATP2A1,

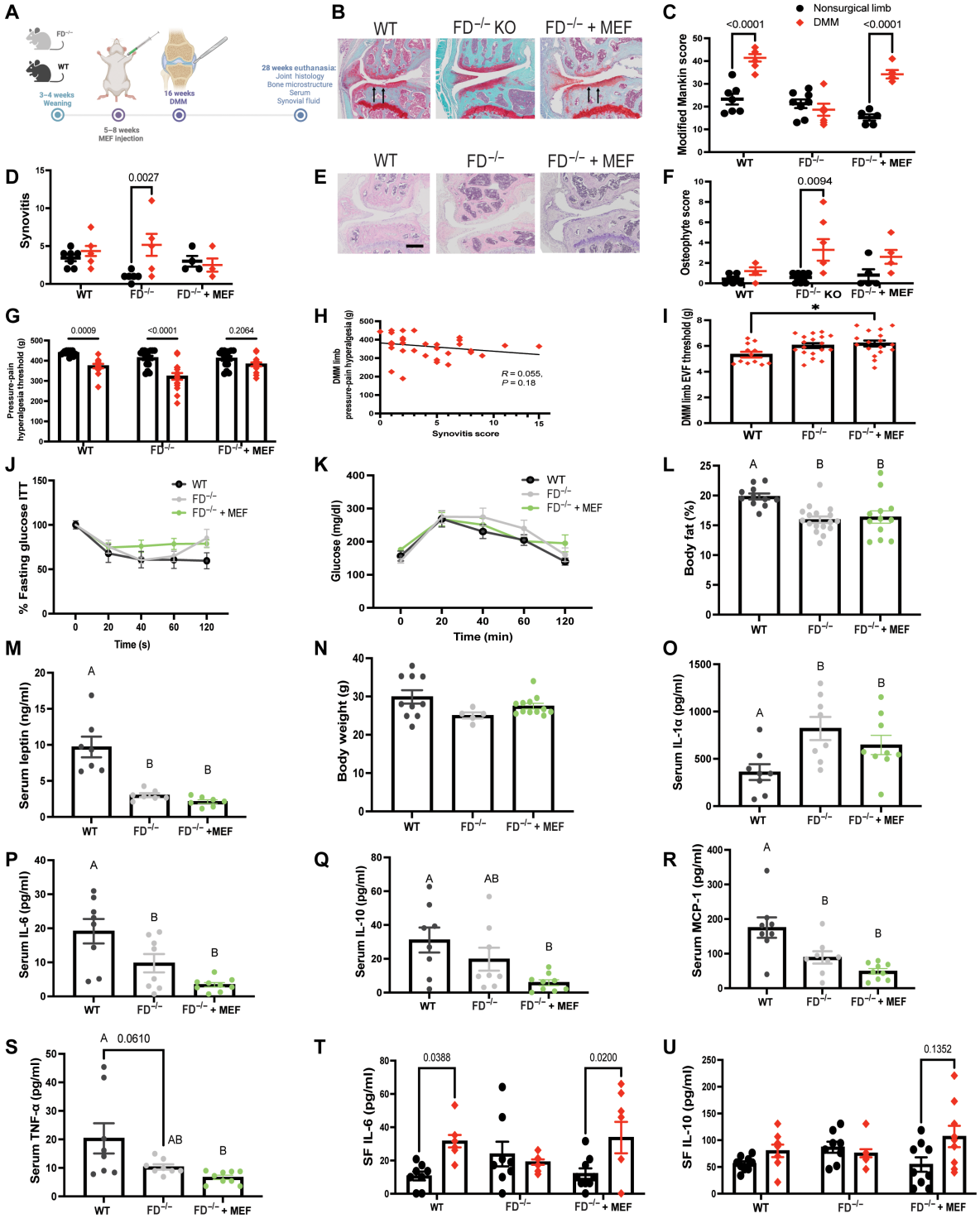


**Fig. 6. FD is a key mediator in the development of OA and joint pain with DMM.** (**A**) Experimental design, (**B**) medial tibial plateau images for Saf-O/Fast Green, and (**C**) knee joint structural damage assessed by modified Mankin score. The scale bar indicates 400 μm. (**D**) Synovitis score, (**E**) synovitis images stained with hematoxylin & eosin, and (**F**) osteophyte scores. Pain measurements included (**G**) pressure-pain hyperalgesia at the knee, which were not explained by (**H**) synovitis and (**I**) Electronic Von Frey. There were no differences in (**J**) insulin tolerance or (**K**) glucose tolerance. (**L**) Body fat, (**M**) serum leptin, and (**N**) body weight. Serum levels for (**O**) IL-1α, (**P**) IL-6, (**Q**) IL-10, (**R**) MCP-1, and (**S**) TNF-α. SF levels for (**T**) IL-6 and (**U**) IL-10. $n = 6$ to 12 per group. Data were analyzed by one-, two-, or three-way ANOVA with Tukey, Sidak, or Bonferroni post hoc tests. Black, nonsurgical limb; red, DMM limb. Different letters indicate $P < 0.05$, or the exact $P$ value is shown for pairwise comparisons. Abbreviations: $FD^{-/-}$, FD KO mice; $FD^{-/-}$ + MEF, $FD^{-/-}$ mice with MEF correction to restore FD; WT, control mice.

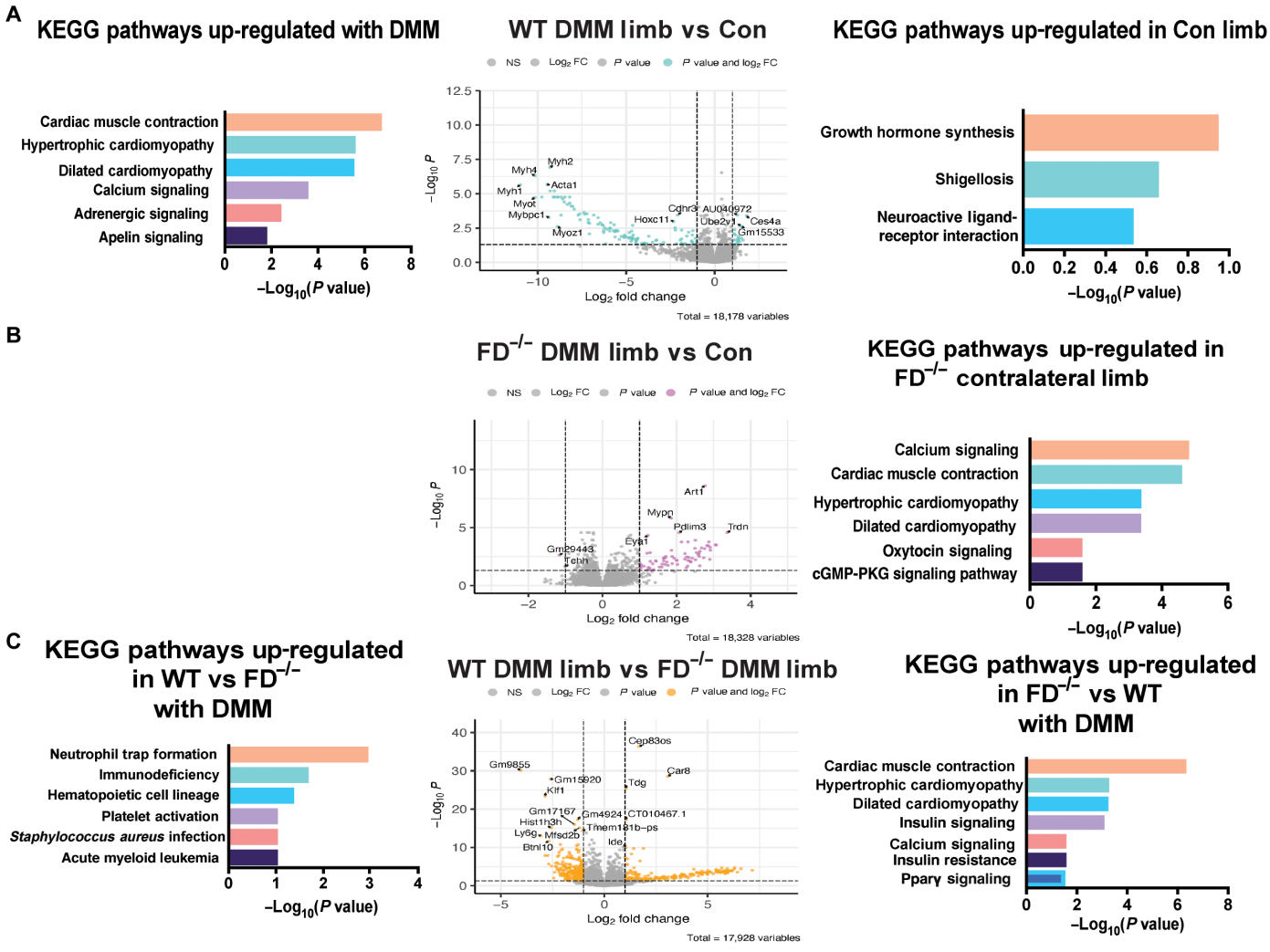


**Fig. 7. Dorsal root ganglia neurons demonstrate differential gene expression with DMM, and in FD-/- compared to WT.** (**A**) KEGG pathways up-regulated in DRGs from nerves that innervate DMM limbs compared to DRGs that innervate non-DMM limbs (left), volcano plot (middle), and KEGG pathways up-regulated in contralateral limb (right). (**B**) No KEGG pathways were up-regulated between the $FD^{-/-}$ DMM limb and the $FD^{-/-}$ contralateral limb because only two genes were up-regulated in $FD^{-/-}$ DMM limbs, as demonstrated in the volcano plot (middle). KEGG pathways up-regulated in the $FD^{-/-}$ contralateral limb versus DMM limb (right). (**C**) KEGG pathways up-regulated in WT DMM versus $FD^{-/-}$ DMM (left), volcano plot comparing WT DMM limb versus $FD^{-/-}$ DMM limb, and KEGG pathways up-regulated in $FD^{-/-}$ DMM versus WT DMM.

CACNA1S, COX6A2, COX7A1, TRDN, and MYH7. These findings indicate potential differences in DRG neuron excitability and neutrophils that may help explain the increased pressure-pain hyperalgesia phenotype exhibited by $FD^{-/-}$ mice.

## DISCUSSION

It is well established that obesity-induced metabolic dysfunction can influence OA, but it has been less appreciated that adipose tissue and the adipokines it releases may play a more direct causative role (*8*). Traditionally, adipokines have not been linked to OA pain, but hand pain was recently associated with elevated leptin levels in patients who are obese with a higher body mass index (*35*). Leptin is also associated with end-stage hip and knee OA pain (*36*), but a causal relationship has not been directly shown. Our studies directly illustrate that systemic adipose-derived leptin is involved in the onset of pain in preclinical OA models and identify the link between alternative pathway FD, cartilage damage, and pain in mice.

Our results showcase a central role of leptin in fat-joint cross-talk for OA development as a minimal level of leptin provided by MEF-HET implants was sufficient to reverse the protected OA phenotype, hyperalgesia, and increased synovitis in LD mice. Although leptin has a well-established influence on metabolism, MEF-KO implants only partially reversed insulin resistance and did not affect glucose tolerance or liver mass, suggesting that the OA phenotype is more responsive to a low level of leptin.

Unexpectedly, MEF implants did not modulate the local synovial inflammatory cytokine content of LD mice with DMM, as measured by the multiplex cytokine array. However, these results may reflect the limitation and sensitivity of this assay in mice. Moreover, sampling and profiling of SF in mouse knee joints were performed at 12 weeks post-DMM and may not be representative of

the inflammation in synovial joint tissues. These findings prompted us to explore the joint milieu using more unbiased and sensitive -omic approaches.

In addition, we observed osteophyte formation in the LD mice in the absence of advanced cartilage damage. We reasoned that the combinatorial effects of increased systemic inflammation and the measured levels of pro-inflammatory mediators in the knee joints of DMM limbs might have contributed to osteophytes observed in these studies. These factors, combined with the cross-talk between leptin and the immune system (*37*), could play a role in bone remodeling (*38*) and, by extension, osteophytosis in the presence and absence of leptin. These speculations remain to be directly tested. Nonetheless, these findings are consistent with our previous work and recent studies that support the notion that systemic adipose tissue drives OA in mice (*8*, *13*).

A recent study found that exogenously increasing circulating leptin levels using an osmotic pump in female rats (*39*) for 23 weeks also altered various systemic and local inflammatory mediators in addition to increased OA damage (*39*), although pain-related behaviors were not measured. For example, we observed that serum IL-17a increased following leptin repletion. Previous studies have demonstrated that IL-17a can up-regulate expression of adipokines and sensitize neurons, but its precise role in the development of pain with fat-joint-DRG cross-talk is unclear (*40*–*42*). We found that saline-treated LD mice had nominally increased DMM damage compared to untreated LD mice, albeit less than leptin-treated LD mice or WT mice with DMM. This damage could result from low-level inflammatory changes in LD mice described here and previously (*8*), or it is possible that the osmotic pump implantation also influences the inflammatory environment.

Data from our exploratory parabiosis experiments support the notion that a soluble factor secreted from adipose tissue was responsible for cartilage fibrillation and proteoglycan loss following DMM. This conclusion is based on the observation, in this limited dataset, that the LD knee joint demonstrated no obvious reconstitution of infrapatellar fat pads and there was no evidence of migration of adipocytes to the knee joints despite sharing circulation with a WT mouse with normal adipose tissue (*8*). Nonetheless, these parabiotic LD mice demonstrated reversal from cartilage protection, similar to that observed with mice receiving MEF-HET and MEF-WT implants. The knees of these mice showed the DMM-induced OA phenotype of fibrillation and proteoglycan loss, suggesting that leptin signaling from WT adipose tissue led to the release of a soluble mediator that acts on the distal peripheral LD joint.

We used transcriptomic characterization of MEF fat pads and multiomic profiling of MEF implant secretomes to search for this leptin-regulated soluble mediator. We observed that FD was the most differentially regulated protein in MEF-sufficient implants and implant secretomes compared to leptin-deficient MEF implants and implant secretomes, suggesting that leptin and FD are tightly co-regulated in adipose tissue, perhaps through the signaling of Pparγ, the master regulator of adipogenesis. Spatial transcriptomics also revealed that FD expression overlapped with the adiponectin-positive regions in the infrapatellar fat pads of nonsurgical WT limbs in the isochronic parabiosis experiment but was evident only in the bone marrow in the DMM limb of LD mice paired with WT. This complex relationship, and the possibility that bone marrow adipokines may influence the onset and progression of OA, remains to be elucidated (*43*).

While a previous study has demonstrated that leptin and FD are both associated with OA progression (*23*), the relationship between leptin and FD and upstream regulation has not been fully explored (*22*, *27*, *28*). We demonstrated that a combined challenge of leptin and lipopolysaccharide induced increased inflammation using primary BMMϕ's, which is consistent with a previous study (*34*). We then demonstrated that BMMϕ's that lack FD have a marked reduction in this inflammation, suggesting that FD is a key downstream mediator of leptin. However, it is not clear whether the macrophage is the key downstream target cell of fat-secreted leptin or complement factors. These data suggest that there could also be a bidirectional feedback loop between leptin and FD that remains to be clarified in future studies. Future work will investigate this directly using spatial transcriptomic approaches.

One potential co-regulator for both leptin and FD is PPARγ, which was significantly up-regulated with DMM and in DRG neurons from $FD^{-/-}$ mice, coinciding with increased pain. PPARγ is a nuclear receptor involved in lipid storage and metabolism. The role of leptin in PPARγ expression has been extensively studied (*44*). PPARγ also regulates the expression of FD (*45*), thus providing a potential mechanistic link between leptin and FD activity that may be explored in future studies. Whether FD is downstream of leptin and whether other regulators of both leptin and FD exist remain to be determined.

The complement cascade has also been shown to influence neuroinflammation, nociception, and musculoskeletal pain (*46*) as genetic deletion of C3 or C5, as well as pharmacologic inhibition of the C3a receptor (C3aR) or C5a receptor 1 (C3aR1), can alleviate hyperalgesia (*47*). Unexpectedly, we observed a heightened pain phenotype in the FD-deficient mice post-DMM that was not explained by synovial inflammation, suggesting that FD plays a role in pain maintenance in DMM-induced OA. Adding FD back to $FD^{-/-}$ DMM mice via MEF-WT implantation significantly increased pain tolerance without affecting insulin or glucose tolerance, affecting body fat, or increasing leptin. Unlike leptin ablation, which reduced IL-17a levels concordant with pain mitigation, $FD^{-/-}$ and repletion of FD did not affect circulating IL-17a levels in serum, suggesting that the pain in $FD^{-/-}$ mice could be independent of IL-17a signaling. Within the DMM joints, coincident with the introduction of cartilage damage, we observed increased IL-6 in SF. There are mixed reports of the role of IL-6 in cartilage degradation with obesity. For example, IL-6 does not necessarily play a direct role in cartilage and meniscus catabolism with obesity (*48*). However, leptin secreted by adipose tissue with obesity may play a role in the cross-talk between synovial fibroblasts and chondrocytes, leading to greater intraarticular IL-6 on patients with OA and obesity (*49*), and SF IL-6 production has been linked to focal cartilage damage in patients with symptomatic OA (*50*). How alternative complement signaling may also regulate intraarticular IL-6, and whether these pathways are directly related to the induction of cartilage damage and pain, remain to be clarified.

Recently, it was demonstrated that nerve repair involves adipose tissue–derived leptin receptor signaling in Schwann cells, indicating that leptin may communicate catabolic process information that confers nerve repair following a nerve crush injury (*51*). Energetic deficiency, or a change in energy balance, in mice lacking leptin receptors can also contribute to neurodegeneration and changes in sensory perception (*52*). Future work will directly validate these targets in the context of OA structural damage and pain.

It is important to note that this study focused on male mice in the MEF experiments, as we previously demonstrated that both male and female LD mice were protected from cartilage damage and pain with DMM. Therefore, male mice were chosen for the studies herein to minimize the number of experimental animals (*8*). Furthermore, the present analysis focused on cross-sectional evaluation of data at euthanasia. Future studies will evaluate female and male mice over several time points postinjury, and during the progression of OA, to better understand the relationship between leptin, FD, OA, and sex of the animals. Last, we are unable to disentangle the relative roles of the infrapatellar fat pad from adipose tissue outside the joint in these studies. Recent studies have demonstrated mixed results about the role of the infrapatellar fat pad in fat-joint cross-talk (*13*, *53*), and our future work aims to directly address this question, especially given the strong transcriptomic signature of FD in this tissue in our spatial transcriptomic studies.

In conclusion, our study provides evidence that leptin secreted by adipose outside of the knee joint contributes to OA in a manner that is independent of global metabolic changes. Previously, it was not possible to disentangle the precise roles of leptin and FD to identify the links we show in the present studies. Our findings suggest a causative link between leptin and FD signaling in the onset of pain in a preclinical model of OA through serum and DRG bulk sequencing analysis, recapitulating a clinically important phenotype of increased hyperalgesia in the absence of cartilage structural damage in individuals with OA and obesity (*54*, *55*). Therefore, this work has several examples of important innovations that are relevant to the fields of orthopedics, rheumatology, aging, obesity, and pain. Our goal was to precisely and specifically target this mechanism to understand the mechanistic link between fat, the knee joint, and pain. There are a few major innovations that are important to the new field of fat-joint cross-talk. These include, first, the direct demonstration that systemic adipose-derived leptin is involved in the onset of pain in preclinical OA models. This is potentially applicable to other painful diseases of metabolic derangement that uniquely target the musculoskeletal system. While it is appreciated that many patients suffer from metabolic derangement (*9*), OA is still considered a focal disease of the joint when the data presented here substantiate that OA could have origins from adipose tissue outside of the knee joint that are transduced to the knee joint. We further demonstrate a link between leptin and FD using a completely unbiased approach, confirming previous correlative relationships, and including pain assays in all our experiments to consider pain and structure in this cross-talk. We then perform exploratory analyses to support the notion that a soluble mediator secreted by fat, rather than reconstitution of the fat pad or a migrating cell population, is likely transducing fat cross-talk to the joint. Last, we identify FD in a completely unbiased way using a novel dual extraction technique to profile both the proteome and metabolome of secreted factors by fat. Our data demonstrate that leptin may signal through innate immune pathways, like the alternative complement pathway, to differentially confer pain and drive cartilage damage, but the exact mechanism remains to be elucidated. This corresponds well with our spatial data that FD is focally in the infrapatellar fat pad and the role for FD in knee joint pain, which is separable from the structure.

We propose that the $FD^{-/-}$ mouse model can be used to further dissect the clinical discordance observed between subjective pain and objective joint structural damage in both OA and obesity-induced OA, which represents a major advance and potential research tool to find new drug targets for OA pain. Together, these data provide a new fundamental mechanistic link of interorgan fat-joint cross-talk that can be harnessed for therapeutic purpose.

## METHODS

### Animal studies

All experimental procedures were approved by the Washington University School of Medicine Department of Comparative Medicine Institutional Animal Care and Use Committee (WUSTL IACUC 22-0306) and were conducted in accordance with ARRIVE guidelines. LD mice and WT [diphtheria toxin A (DTA)/+] littermate controls were generated for these studies by crossing adiponectin-Cre (the Jackson Laboratory, 028020) mice with homozygous lox-stop-lox-ROSA-DTA (the Jackson Laboratory, 010527) mice on a C57BL/6 background. To breed at Mendelian frequency, mice were bred and maintained at thermoneutrality throughout their lifespan (30°C) (*8*, *26*). Mixed genotype mice were group housed such that $n = 3$ to 5 per cage.

Male LD mice received either a MEF transplant (MEF-rescue) from WT, leptin heterozygous (MEF-HET), or leptin homozygous KO (MEF-KO) pups, as previously described, which developed into adipose-like tissue (*12*, *29*) between 3 and 5 weeks of age. The injection was delivered subcutaneously to the sternal aspect of a donor LD mouse (3 to 5 weeks old) under 2% isoflurane with a 27-gauge needle. Animal numbers used in each experiment can be found in the figure legend.

### Exogenous leptin delivery

Osmotic pumps were surgically implanted to the dorsal aspect of mice at 15 weeks of age, 1 week before DMM. Leptin or saline was delivered to LD mice using Azlet 2006 (Cupertino, CA) at a release rate of 0.15 μl/hour to deliver a total of 1 mg of leptin over 6 weeks, and the osmotic pumps were replaced with new, sterile implants until 28 weeks of age. The leptin concentration was confirmed after implantation.

### OA induction by DMM

At 16 weeks of age, surgical animals underwent DMM surgery in their left knee joints, and the right limb served as a nonsurgical contralateral control. Behavioral and metabolic assays were conducted throughout the course of this study. Mice were euthanized at 28 weeks of age to assess OA severity, bone microstructure, and serum and SF inflammatory profiles. Knee joints were fixed in 4% paraformaldehyde and decalcified in 10% formic acid (Cal-Ex II) for 48 to 72 hours. Histological assessment was performed by modified Mankin scoring, synovitis scoring, and osteophyte scoring on formalin-fixed, paraffin-embedded 5-μm sections, as previously described (*8*). Bone marrow adipocytes were counted in ImageJ on histological sections.

### Body composition, tissue harvest, and storage

Mice were weighed weekly throughout the course of the study using a standard scale (grams). Body fat was measured by DXA (Lunar Piximus) at 27 weeks of age to quantify body fat. Animals were euthanized at 28 weeks of age in accordance with the timelines in each figure. Body mass, liver mass, body fat, blood, L3-L5 DRG sensory neurons from $FD^{-/-}$ and WT mice, and SF were harvested.

### Serum and Synovial Fluid profiling

All mice were fasted overnight before euthanasia. Serum was collected in a BD Microtainer STT serum separator tube and allowed to

clot at room temperature. SF was collected using an alginate pad that was digested in alginate lyase until a stop solution was applied (*8*, *56*, *57*). Both fluids were stored at −80°C until analysis by Luminex multiplex 18-plex chemokine/cytokine array assay (Eve Technologies) (*8*). ELISA for serum leptin was conducted using a mouse/rat Leptin Quantikine ELISA Assay kit (MOB00; R&D Systems) at a dilution of 1:2 in LD mice, and all other groups were evaluated at the manufacturer's recommended 1:20 dilution.

### Bone microstructure analysis

Whole knee joints were scanned by microCT (Bruker SkyScan1176) at an 18-μm isotropic voxel resolution according to previously reported methods (*8*, *56*, *57*). To reduce beam hardening, a 0.5-mm aluminum filter was used during scanning. Hydroxyapatite calibration phantoms were scanned to calibrate bone density. Scans were reconstructed to three-dimensional images using NRecon software, and CTAn software was used to segment subchondral and trabecular regions from the medial tibial plateau, lateral tibial plateau, medial femoral condyle, and lateral femoral condyle for analysis. The tibial epiphysis was identified using the subchondral plate and growth plate as references. The tibial metaphysis was defined as the 1-mm area directly below the growth plate. The main outcomes reported from microCT images are BMD, BV/TV (%), trabecular number, and trabecular thickness.

### Insulin and glucose tolerance tests

Insulin and glucose tolerance tests were performed 4 weeks post-DMM surgery (20 weeks of age) after fasting mice for a minimum of 4 hours. Each test was conducted at least 1 week apart in all animals. For both tests, fasting glucose levels were measured by tail bleed at time point 0 to establish a baseline. For glucose tolerance tests, animals were administered 10% dextrose (1 mg/kg; 1% volume/body mass) by intraperitoneal injection, and for insulin tolerance tests, 0.75 U/kg body mass of insulin (Humulin R diluted to 75 mU/ml, 1% volume/body mass) was administered by intraperitoneal injection (*8*, *12*). Serial blood glucose measurements were taken via tail vein at 20, 40, 60, and 120 min after injection with a glucose meter (Contour; Bayer).

### Pain assessments and behavioral testing

All animals were acclimatized to all equipment 1 day before the onset of testing. Two measures for pain were conducted at 27 weeks of age. To assess tactile allodynia in the DMM limb, an Electronic Von Frey assay was used as previously described (*8*). Hind paws of DMM limbs were stimulated three to five times. The intensity of the stimulus (grams) was recorded by the tester when the paw was withdrawn. To assess mechanical hyperalgesia, pressure-pain tests were conducted using a small animal algometer (SMALGO; Bioseb) (*8*). Three to five trials of the surgical and nonsurgical limbs were collected by applying a steadily increasing force to the lateral aspect of each limb until the limb was withdrawn. The average of three trials for each limb was reported, and a maximum value of 450 g was used to avoid tissue damage to the knee joint.

### Isochronic parabiosis

Female LD and WT littermates were housed as a pair from weaning until 8 to 10 weeks of age, where we performed isochronic parabiosis (*58*). At 16 weeks, the LD mouse was challenged with DMM surgery unilaterally on their left outside limb. Mice were monitored for 12 weeks and euthanized at 28 weeks of age. Sera and hindlimbs were collected for further analysis.

### Spatial transcriptomics and knee joint assessment

Samples were fixed in 4% paraformaldehyde for 24 hours from mice that were joined by isochronic parabiosis. A reduced decalcification time of 10 hours at 4°C on an orbital shaker was used for knee joints. Joint tissues were processed according to previous protocols and cut on a Leica Microtome at 5 μm. Serial sections were used for staining with hematoxylin and eosin and toluidine blue/oil red O and an unstained slide onto Fisher Superfrost Plus slides or Dako Flex IHC adhesive slides and prepared for spatial transcriptomics by 10x Visium using the standard CytAssist protocol. The concentration of each library was accurately determined through quantitative polymerase chain reaction using the KAPA library Quantification Kit according to the manufacturer's protocol (KAPA Biosystems/Roche) to produce cluster counts appropriate for the Illumina NovaSeq6000 instrument. Normalized libraries were sequenced on a NovaSeqX 10B or NovaSeq6000 S4 Flow Cell using the 151 × 10 × 10 × 151 sequencing recipe according to the manufacturer's protocol. Read 1 was trimmed to the 10x Genomics recommendation of 28 base pairs. A median sequencing depth of 50,000 reads per cell was targeted for each gene expression library. The data were then spatially analyzed using standard graph-based clustering methods and visualized using 10x Space Ranger and 10x Loupe browser version 7.

### Adipose and Dorsal Root Ganglion bulk RNA-seq

Total RNA integrity was determined using an Agilent Bioanalyzer. Library preparation was performed with 500 ng of total RNA. Ribosomal RNA was removed by a ribonuclease H method using RiboErase kits (Kapa Biosystems). mRNA was then fragmented in reverse transcriptase buffer and heated to 94°C for 8 min. mRNA was reverse transcribed to yield cDNA using SuperScript III RT enzyme (Life Technologies, per the manufacturer's instructions) and random hexamers. A second strand reaction was performed to yield double-stranded cDNA. cDNA was blunt ended, had an A base added to the 3′ ends, and then had Illumina sequencing adapters ligated to the ends. Ligated fragments were then amplified for 16 cycles using primers incorporating unique dual index tags. Fragments were sequenced on an Illumina NovaSeq-6000 using paired end reads extending 150 bases. Basecalls and demultiplexing were performed with Illumina's bcl2fastq software with a maximum of one mismatch in the indexing read. RNA-seq reads were then aligned to the Ensembl release 101 primary assembly with STAR version 2.7.9a1. Gene counts were derived from the number of uniquely aligned unambiguous reads by Subread:featureCount version 2.0.32. Isoform expression of known Ensembl transcripts was quantified with Salmon version 1.5.23. Sequencing performance was assessed for the total number of aligned reads, total number of uniquely aligned reads, and features detected. The ribosomal fraction, known junction saturation, and read distribution over known gene models were quantified with RSeQC version 4.04.

### RNA-seq data processing

RNA-seq data were processed as in a previous study (*59*). RNA-seq data of mouse ganglia were processed by Cutadapt (version 2.7; --quality-cutoff=15,10 --minimum-length=36) to remove adapters and FastQC (version 0.11.4) to estimate the sequencing quality. Trimmed reads were then aligned to the mouse genome mm10 with

GENCODE annotation vM28 using STAR (version 2.5.4) with default parameters (*60*). Transcript quantification was performed using featureCounts from the subread package (version 1.6.3) (*61*). Sequencing performance was assessed for the total number of aligned reads, total number of uniquely aligned reads, and features detected. The ribosomal fraction, known junction saturation, and read distribution over known gene models were quantified with RSeQC version 2.6.2 (*62*). Principal components analysis and differential expression analysis were performed using DESeq2 in negative binomial mode using batch-corrected transcripts from featureCounts (greater than twofold expression change, >1 count per million, Benjamini-corrected $P < 0.05$). Pairwise comparisons were made between groups to determine differentially expressed genes within each group. Gene ontology and KEGG analyses were performed using EnrichR for differentially expressed genes (*63*). The gene expression was plotted using ggplot2 and pheatmap. Statistical analysis was performed using R.

### Metabolomics and proteomics

Fat was explanted, weighed, washed, and filtered, and 100 mg was prepared for bulk sequencing ($n = 3$ to 5 per group), while 250 mg was cultured for 24 hours in 1% Dulbecco's modified Eagle's medium. The resulting CM were collected and compared to CM derived from naïve WT fat of equal mass (250 mg) ($n = 4$ to 8 per group). CM protein and metabolites were extracted and evaluated via liquid chromatography–mass spectrometry (*64*). Significant metabolites and protein intensities were detected using clustering and false discovery rate corrections in MetaboAnalyst ($P < 0.05$). Data were log transformed and compared using hierarchical cluster analysis, volcano plot analysis, principal components analysis, PLS-DA, and variable importance in projection scores. Median intensity heatmaps were calculated in MATLAB to determine features uniquely up-regulated in each group. Integrated metabolomic and proteomic pathway impact analysis was conducted in MetaboAnalyst using UniProt and KEGG identifications.

### Statistical analysis

Graphing and analysis were performed in GraphPad Prism 10 (GraphPad Software). A priori α was defined as 0.05. Data were evaluated for normality using a Shapiro-Wilk test and Levene's test for equal variance. Statistical analysis and the number of animals per group for each experiment are described in each figure legend. Data are presented as the means ± SE and were compared by either one-way, two-way (group × limb; genotype × sex; genotype × diet), or three-way (limb × genotype × diet; limb × genotype × sex) ANOVA with Dunnett's, Sidak, or Tukey's post hoc test.

## Supplementary Materials

**This PDF file includes:**

Supplementary Methods
Figs. S1 to S8
Tables S1 to S4

## REFERENCES AND NOTES


1. T. M. Griffin, J. L. Huebner, V. B. Kraus, Z. Yan, F. Guilak, Induction of osteoarthritis and metabolic inflammation by a very high-fat diet in mice: Effects of short-term exercise. *Arthritis Rheum.* **64**, 443–453 (2012).
2. R. F. Loeser, S. R. Goldring, C. R. Scanzello, M. B. Goldring, Osteoarthritis: A disease of the joint as an organ. *Arthritis Rheum.* **64**, 1697–1707 (2012).
3. A.-M. Malfait, Why we should study pain in animal models of rheumatic diseases. *Clin. Exp. Rheumatol.* **35**, 37–39 (2017).
4. E. Sebbag, R. Felten, F. Sagez, J. Sibilia, H. Devilliers, L. Arnaud, The world-wide burden of musculoskeletal diseases: A systematic analysis of the World Health Organization Burden of Diseases Database. *Ann. Rheum. Dis.* **78**, 844–848 (2019).
5. G. A. Hawker, Osteoarthritis is a serious disease. *Clin. Exp. Rheumatol.* **37**, 3–6 (2019).
6. F. Berenbaum, I. J. Wallace, D. E. Lieberman, D. T. Felson, Modern-day environmental factors in the pathogenesis of osteoarthritis. *Nat. Rev. Rheumatol.* **14**, 674–681 (2018).
7. T. M. Griffin, J. L. Huebner, V. B. Kraus, F. Guilak, Extreme obesity due to impaired leptin signaling in mice does not cause knee osteoarthritis. *Arthritis Rheum.* **60**, 2935–2944 (2009).
8. K. H. Collins, K. L. Lenz, E. N. Pollitt, D. Ferguson, I. Hutson, L. E. Springer, A. K. Oestreich, R. Tang, Y. R. Choi, G. A. Meyer, S. L. Teitelbaum, C. T. N. Pham, C. A. Harris, F. Guilak, Adipose tissue is a critical regulator of osteoarthritis. *Proc. Natl. Acad. Sci. U.S.A.* **118**, e2021096118 (2021).
9. M. Binvignat, J. Sellam, F. Berenbaum, D. T. Felson, The role of obesity and adipose tissue dysfunction in osteoarthritis pain. *Nat. Rev. Rheumatol.* **20**, 565–584 (2024).
10. C. R. Kahn, G. Wang, K. Y. Lee, Altered adipose tissue and adipocyte function in the pathogenesis of metabolic syndrome. *J. Clin. Invest.* **129**, 3990–4000 (2019).
11. X. Zhang, H. Robles, K. L. Magee, M. R. Lorenz, Z. Wang, C. A. Harris, C. S. Craft, E. L. Scheller, A bone-specific adipogenesis pathway in fat-free mice defines key origins and adaptations of bone marrow adipocytes with age and disease. *eLife* **10**, e66275 (2021).
12. K. H. Collins, C. Gui, E. V. Ely, K. L. Lenz, C. A. Harris, F. Guilak, G. A. Meyer, Leptin mediates the regulation of muscle mass and strength by adipose tissue. *J. Physiol.* **600**, 3795–3817 (2022).
13. J. J. McClure, G. D. McIlroy, R. A. Symons, S. M. Clark, I. Cunningham, W. Han, K. Kania, F. Colella, J. J. Rochford, C. De Bari, A. J. Roelofs, Disentangling the detrimental effects of local from systemic adipose tissue dysfunction on articular cartilage in the knee. *Osteoarthr. Cartil.* **32**, 1552–1565 (2024).
14. Y. H. Gao, C. W. Zhao, B. Liu, N. Dong, L. Ding, Y. R. Li, J. G. Liu, W. Feng, X. Qi, X. H. Jin, An update on the association between metabolic syndrome and osteoarthritis and on the potential role of leptin in osteoarthritis. *Cytokine* **129**, 155043 (2020).
15. F. Berenbaum, T. M. Griffin, R. Liu-Bryan, Metabolic regulation of inflammation in osteoarthritis. *Arthritis Rheumatol.* **69**, 9–21 (2017).
16. T. M. Griffin, B. Fermor, J. L. Huebner, V. B. Kraus, R. M. Rodriguiz, W. C. Wetsel, L. Cao, L. A. Setton, F. Guilak, Diet-induced obesity differentially regulates behavioral, biomechanical, and molecular risk factors for osteoarthritis in mice. *Arthritis Res. Ther.* **12**, R130 (2010).
17. N. K. Y. Wee, T. F. C. de Lima, N. E. McGregor, E. C. Walker, I. J. Poulton, M. Blank, N. A. Sims, Leptin receptor in osteocytes promotes cortical bone consolidation in female mice. *J. Endocrinol.* **255**, 25–37 (2022).
18. O. Malaise, B. Relic, E. Charlier, M. Zeddou, S. Neuville, C. Deroyer, P. Gillet, E. Louis, M. G. Malaise, D. de Seny, Glucocorticoid-induced leucine zipper (GILZ) is involved in glucocorticoid-induced and mineralocorticoid-induced leptin production by osteoarthritis synovial fibroblasts. *Arthritis Res. Ther.* **18**, 219 (2016).
19. B. O. Zhou, R. Yue, M. M. Murphy, J. G. Peyer, S. J. Morrison, Leptin-receptor-expressing mesenchymal stromal cells represent the main source of bone formed by adult bone marrow. *Cell Stem Cell* **15**, 154–168 (2014).
20. R. Gandhi, M. Takahashi, C. Virtanen, K. Syed, J. R. Davey, N. N. Mahomed, Microarray analysis of the infrapatellar fat pad in knee osteoarthritis: Relationship with joint inflammation. *J. Rheumatol.* **38**, 1966–1972 (2011).
21. K. T. Chang, Y. L. Lin, C. T. Lin, M. J. Tsai, W. C. Huang, Y. H. Shih, Y. Y. Lee, H. Cheng, M. C. Huang, Data on the expression of leptin and leptin receptor in the dorsal root ganglion and spinal cord after preganglionic cervical root avulsion. *Data Brief* **15**, 567–572 (2017).
22. G. Valverde-Franco, G. Tardif, F. Mineau, F. Paré, B. Lussier, H. Fahmi, J. P. Pelletier, J. Martel-Pelletier, High in vivo levels of adipsin lead to increased knee tissue degradation in osteoarthritis: Data from humans and animal models. *Rheumatology (Oxford)* **57**, 1851–1860 (2018).
23. J. Martel-Pelletier, J. P. Raynauld, M. Dorais, F. Abram, J. P. Pelletier, The levels of the adipokines adipsin and leptin are associated with knee osteoarthritis progression as assessed by MRI and incidence of total knee replacement in symptomatic osteoarthritis patients: A post hoc analysis. *Rheumatology (Oxford)* **55**, 680–688 (2016).
24. Q. Wang, A. L. Rozelle, C. M. Lepus, C. R. Scanzello, J. J. Song, D. M. Larsen, J. F. Crish, G. Bebek, S. Y. Ritter, T. M. Lindstrom, I. Hwang, H. H. Wong, L. Punzi, A. Encarnacion, M. Shamloo, S. B. Goodman, T. Wyss-Coray, S. R. Goldring, N. K. Banda, J. M. Thurman, R. Gobezie, M. K. Crow, V. M. Holers, D. M. Lee, W. H. Robinson, Identification of a central role for complement in osteoarthritis. *Nat. Med.* **17**, 1674–1679 (2011).
25. S. Rafail, I. Kourtzelis, P. G. Foukas, M. M. Markiewski, R. A. DeAngelis, M. Guariento, D. Ricklin, E. A. Grice, J. D. Lambris, Complement deficiency promotes cutaneous wound healing in mice. *J. Immunol.* **194**, 1285–1291 (2015).

26. X. Wu, I. Hutson, A. M. Akk, S. Mascharak, C. T. N. Pham, D. E. Hourcade, R. Brown, J. P. Atkinson, C. A. Harris, Contribution of adipose-derived factor D/adipsin to complement alternative pathway activation: Lessons from lipodystrophy. *J. Immunol.* **200**, 2786–2797 (2018).
27. J. S. Flier, K. S. Cook, P. Usher, B. M. Spiegelman, Severely impaired adipsin expression in genetic and acquired obesity. *Science* **237**, 405–408 (1987).
28. F. Paré, G. Tardif, H. Fahmi, Y. Ouhaddi, J. P. Pelletier, J. Martel-Pelletier, *In vivo* protective effect of adipsin-deficiency on spontaneous knee osteoarthritis in aging mice. *Aging (Albany NY)* **12**, 2880–2896 (2020).
29. D. Ferguson, M. Blenden, I. Hutson, Y. Du, C. A. Harris, Mouse embryonic fibroblasts protect ob/ob mice From obesity and metabolic complications. *Endocrinology* **159**, 3275–3286 (2018).
30. E. Kozhemyakina, M. Zhang, A. Ionescu, U. M. Ayturk, N. Ono, A. Kobayashi, H. Kronenberg, M. L. Warman, A. B. Lassar, Identification of a Prg4-expressing articular cartilage progenitor cell population in mice. *Arthritis Rheumatol.* **67**, 1261–1273 (2015).
31. J. Martel-Pelletier, G. Tardif, J. R. Trépanier, F. Abram, M. Dorais, J.-P. Raynauld, J.-P. Pelletier, The ratio adipsin/MCP-1 is strongly associated with structural changes and CRP/MCP-1 with symptoms in obese knee osteoarthritis subjects: Data from the Osteoarthritis Initiative. *Osteoarthr. Cartil.* **27**, 1163–1173 (2019).
32. A. V. Perruccio, N. N. Mahomed, V. Chandran, R. Gandhi, Plasma adipokine levels and their association with overall burden of painful joints among individuals with hip and knee osteoarthritis. *J. Rheumatol.* **41**, 334–337 (2014).
33. K. Kiernan, N. J. MacIver, The role of the adipokine leptin in immune cell function in health and disease. *Front. Immunol.* **11**, 622468 (2020).
34. L. B. Monteiro, J. S. Prodonoff, C. Favero de Aguiar, F. Correa-da-Silva, A. Castoldi, N. V. T. Bakker, G. G. Davanzo, B. Castelucci, J. Pereira, J. Curtis, J. Buscher, L. M. D. Reis, G. Castro, G. Ribeiro, J. V. Virgilio-da-Silva, D. Adamoski, S. M. G. Dias, S. R. Consonni, J. Donato, E. J. Pearce, N. O. S. Camara, P. M. Moraes-Vieira, Leptin signaling suppression in macrophages improves immunometabolic outcomes in obesity. *Diabetes* **71**, 1546–1561 (2022).
35. M. Gløersen, P. Steen Pettersen, T. Neogi, S. R. Jafarzadeh, M. Vistnes, C. S. Thudium, A.-C. Bay-Jensen, J. Sexton, T. K. Kvien, H. B. Hammer, I. K. Haugen, Associations of body mass index with pain and the mediating role of inflammatory biomarkers in people with hand osteoarthritis. *Arthritis Rheumatol.* **74**, 810–817 (2022).
36. A. Lubbeke, A. Finckh, G. J. Puskas, D. Suva, A. Ladermann, S. Bas, D. Fritschy, C. Gabay, P. Hoffmeyer, Do synovial leptin levels correlate with pain in end stage arthritis? *Int. Orthop.* **37**, 2071–2079 (2013).
37. D. Ait Eldjoudi, A. Cordero Barreal, M. Gonzalez- Rodríguez, C. Ruiz- Fernández, Y. Farrag, M. Farrag, F. Lago, M. Capuozzo, M. A. Gonzalez-Gay, A. Mera Varela, J. Pino, O. Gualillo, Leptin in osteoarthritis and rheumatoid arthritis: Player or bystander? *Int. J. Mol. Sci.* **23**, 2859 (2022).
38. W. Zou, N. Rohatgi, J. R. Brestoff, Y. Zhang, E. L. Scheller, C. S. Craft, M. D. Brodt, N. Migotsky, M. J. Silva, C. A. Harris, S. L. Teitelbaum, Congenital lipodystrophy induces severe osteosclerosis. *PLOS Genet.* **15**, e1008244 (2019).
39. Y. Fu, A. Batushansky, M. Kinter, J. L. Huebner, V. B. Kraus, T. M. Griffin, Effects of leptin and body weight on inflammation and knee osteoarthritis phenotypes in female rats. *JBMR Plus* **7**, e10754 (2023).
40. F. A. Pinho-Ribeiro, W. A. Verri Jr., I. M. Chiu, Nociceptor sensory neuron-immune interactions in pain and inflammation. *Trends Immunol.* **38**, 5–19 (2017).
41. D. R. Maestas Jr., L. Chung, J. Han, X. Wang, S. D. Sommerfeld, S. H. Kelly, E. Moore, H. H. Nguyen, J. C. Mejias, A. N. Pena, H. Zhang, J. S. T. Hooks, A. F. Chin, J. I. Andorko, C. A. Berlinicke, K. Krishnan, Y. Choi, A. E. Anderson, R. Mahatme, C. Mejia, M. Eric, J. Woo, S. Ganguly, D. J. Zack, L. Zhao, E. J. Pearce, F. Housseau, D. M. Pardoll, J. H. Elisseeff, Helminth egg derivatives as proregenerative immunotherapies. *Proc. Natl. Acad. Sci. U.S.A.* **120**, e2211703120 (2023).
42. S. J. B. Snelling, S. Bas, G. J. Puskas, S. G. Dakin, D. Suva, A. Finckh, C. Gabay, P. Hoffmeyer, A. J. Carr, A. Lübbeke, Presence of IL-17 in synovial fluid identifies a potential inflammatory osteoarthritic phenotype. *PLOS ONE* **12**, e0175109 (2017).
43. T. Hugle, J. Geurts, What drives osteoarthritis?—Synovial versus subchondral bone pathology. *Rheumatology (Oxford)* **56**, 1461–1471 (2017).
44. P. Tontonoz, B. M. Spiegelman, Fat and beyond: The diverse biology of PPARγ. *Annu. Rev. Biochem.* **77**, 289–312 (2008).
45. K. Y. Ryu, E. J. Jeon, J. Leem, J.-H. Park, H. Cho, Regulation of adipsin expression by endoplasmic reticulum stress in adipocytes. *Biomolecules* **10**, 314 (2020).
46. C. A. Warwick, A. L. Keyes, T. M. Woodruff, Y. M. Usachev, The complement cascade in the regulation of neuroinflammation, nociceptive sensitization, and pain. *J. Biol. Chem.* **297**, 101085 (2021).
47. J. Xu, P. Huang, B. Bie, Y. Dai, S. Ben-Salem, N. Borjini, L. Zhang, J. Chen, M. Olman, J. Cheng, F. Lin, Complement receptor C3aR1 contributes to paclitaxel-induced peripheral neuropathic pain in mice and rats. *J. Immunol.* **211**, 1736–1746 (2023).
48. A. L. McNulty, M. R. Miller, S. K. O'Connor, F. Guilak, The effects of adipokines on cartilage and meniscus catabolism. *Connect. Tissue Res.* **52**, 523–533 (2011).
49. M. J. Pearson, D. Herndler-Brandstetter, M. A. Tariq, T. A. Nicholson, A. M. Philp, H. L. Smith, E. T. Davis, S. W. Jones, J. M. Lord, IL-6 secretion in osteoarthritis patients is mediated by chondrocyte-synovial fibroblast cross-talk and is enhanced by obesity. *Sci. Rep.* **7**, 3451 (2017).
50. A. I. Tsuchida, M. Beekhuizen, M. Rutgers, G. J. van Osch, J. E. Bekkers, A. G. Bot, B. Geurts, W. J. Dhert, D. B. Saris, L. B. Creemers, Interleukin-6 is elevated in synovial fluid of patients with focal cartilage defects and stimulates cartilage matrix production in an in vitro regeneration model. *Arthritis Res. Ther.* **14**, R262 (2012).
51. V. K. Sundaram, V. Schütza, N. H. Schröter, A. Backhaus, A. Bilsing, L. Joneck, A. Seelbach, C. Mutschler, J. A. Gomez-Sanchez, E. Schäffner, E. E. Sánchez, D. Akkermann, C. Paul, N. Schwagarus, S. Müller, A. Odle, G. Childs, D. Ewers, T. Kungl, M. Sitte, G. Salinas, M. W. Sereda, K.-A. Nave, M. H. Schwab, M. Ost, P. Arthur-Farraj, R. M. Stassart, R. Fledrich, Adipo-glial signaling mediates metabolic adaptation in peripheral nerve regeneration. *Cell Metab.* **35**, 2136–2152.e9 (2023).
52. M. Leal-Julià, J. J. Vilches, A. Onieva, S. Verdés, Á. Sánchez, M. Chillon, X. Navarro, A. Bosch, Proteomic quantitative study of dorsal root ganglia and sciatic nerve in type 2 diabetic mice. *Mol. Metab.* **55**, 101408 (2022).
53. M. F. Afzali, M. M. Sykes, L. H. Burton, K. M. Patton, K. R. Lee, C. Seebart, N. Vigon, R. Ek, G. E. Narez, A. J. Marolf, K. J. Sikes, T. L. Haut Donahue, K. S. Santangelo, Removal of the infrapatellar fat pad and associated synovium benefits female guinea pigs in the Dunkin Hartley model of idiopathic osteoarthritis. *Ann. Transl. Med.* **12**, 43 (2024).
54. L. C. Carlesso, T. Neogi, Identifying pain susceptibility phenotypes in knee osteoarthritis. *Clin. Exp. Rheumatol.* **37**, 96–99 (2019).
55. L. C. Carlesso, S. R. Jafarzadeh, A. Stokes, D. T. Felson, N. Wang, L. Frey-Law, C. E. Lewis, M. Nevitt, T. Neogi, Multicenter Osteoarthritis Study Group, Depressive symptoms and multi-joint pain partially mediate the relationship between obesity and opioid use in people with knee osteoarthritis. *Osteoarthr. Cartil.* **30**, 1263–1269 (2022).
56. R. Tang, N. S. Harasymowicz, C.-L. Wu, K. H. Collins, Y. R. Choi, S. J. Oswald, F. Guilak, Gene therapy for follistatin mitigates systemic metabolic inflammation and post-traumatic arthritis in high-fat diet–induced obesity. *Sci. Adv.* **6**, eaaz7492 (2020).
57. N. S. Harasymowicz, Y.-R. Choi, C.-L. Wu, L. Iannucci, R. Tang, F. Guilak, Intergenerational transmission of diet-induced obesity, metabolic imbalance, and osteoarthritis in mice. *Arthritis Rheumatol.* **72**, 632–644 (2020).
58. P. Kamran, K. I. Sereti, P. Zhao, S. R. Ali, I. L. Weissman, R. Ardehali, Parabiosis in mice: A detailed protocol. *J. Vis. Exp.*, 50556 (2013).
59. B. Miao, X. Xing, V. Bazylianska, P. Madden, A. Moszczynska, B. Zhang, Methamphetamine-induced region-specific transcriptomic and epigenetic changes in the brain of male rats. *Commun. Biol.* **6**, 991 (2023).
60. A. Dobin, C. A. Davis, F. Schlesinger, J. Drenkow, C. Zaleski, S. Jha, P. Batut, M. Chaisson, T. R. Gingeras, STAR: Ultrafast universal RNA-seq aligner. *Bioinformatics* **29**, 15–21 (2013).
61. Y. Liao, G. K. Smyth, W. Shi, featureCounts: An efficient general purpose program for assigning sequence reads to genomic features. *Bioinformatics* **30**, 923–930 (2014).
62. L. Wang, S. Wang, W. Li, RSeQC: Quality control of RNA-seq experiments. *Bioinformatics* **28**, 2184–2185 (2012).
63. M. V. Kuleshov, M. R. Jones, A. D. Rouillard, N. F. Fernandez, Q. Duan, Z. Wang, S. Koplev, S. L. Jenkins, K. M. Jagodnik, A. Lachmann, M. G. McDermott, C. D. Monteiro, G. W. Gundersen, A. Ma'ayan, Enrichr: A comprehensive gene set enrichment analysis web server 2016 update. *Nucleic Acids Res.* **44**, W90–W97 (2016).
64. H. D. Welhaven, G. Vahidi, S. T. Walk, B. Bothner, S. A. Martin, C. M. Heveran, R. K. June, The cortical bone metabolome of C57BL/6J mice is sexually dimorphic. *JBMR Plus* **6**, e10654 (2022).


**Acknowledgments:** We thank E. Erdogan for initial help with multiomic studies, E. Pollitt for initial help with microCT studies, and S. Dunivan for help with quantifying bone marrow adipose in histology sections. We also thank W. Feng from the Center of Regenerative Medicine at Washington University for bioinformatics support related to bulk sequencing. We thank the Genome Technology Access Center at the McDonnell Genome Institute at Washington University School of Medicine for help with sample preparation, sequencing, and analysis, with special thanks to J. Ponce and B. Delgado. We also acknowledge C. Harris for assistance with the LD mouse model and MEF procedure. **Funding:** This work was supported by the following: Pilot and Feasibility funding from the Washington University School of Medicine Musculoskeletal Research Center P30 (AR074992), C. Idleberg and S. Coleman for histology support, The Washington University in St. Louis Rheumatic Diseases Research Resource-Based Center P30 (AR073752), NIAMS K99/R00 (AR78949) awarded to K.H.C., DP2 awarded to K.H.C. (AG093209), NIAMS K01 awarded to A.K.O. (AR079045), 10x Genomics for in-kind reagents, and M. Ramani for technical support related to the Visium Protocol Development. The GTAC Center is partially supported by NCI Cancer Center Support grant (P30 CA91842) to the Siteman Cancer Center. We are grateful for additional grant support from Shriner's Hospitals for Children–St. Louis, Arthritis National Research Foundation, NIH (AG046927 and AR080902 awarded to F.G.), and Institute of Clinical and Translational Sciences at Washington University in St. Louis Just in Time Grant Program. This publication is solely the responsibility of the authors and does not necessarily represent the official view of NCRR, NIAMS, or NIH. We

acknowledge the help and expertise of D. R. Quilici, R. Woosley, and the Mitch Hitchcock Nevada Proteomics Center, which is supported in part by the Nevada INBRE, a grant from the National Institute of General Medical Sciences within the National Institutes of Health. A Pilot and Feasibility grant was awarded to K.H.C. from the Chicago Center for Musculoskeletal Pain at Rush University (P30 AR079206), which supported the bulk RNA-seq on the DRGs. **Author contributions:** K.H.C.: writing—original draft, conceptualization, investigation, writing—review and editing, methodology, resources, funding acquisition, data curation, validation, supervision, formal analysis, software, project administration, and visualization. K.L.L.: conceptualization, investigation, writing—review and editing, resources, and data curation. H.D.W.: writing—original draft, conceptualization, investigation, writing—review and editing, methodology, resources, data curation, validation, formal analysis, and visualization. E.E.: writing—original draft, investigation, writing—review and editing, methodology, resources, data curation, and validation. L.E.S.: investigation. S.P.: investigation. L.B.: investigation. R.T.: investigation, writing—review and editing, and validation. A.A.: investigation, validation, formal analysis, and visualization. H.Y.: investigation and visualization. B.Z.: investigation. X.W.: investigation, writing—review and editing, methodology, resources, and validation. J.P.A.: conceptualization, investigation, writing—review and editing, methodology, resources, funding acquisition, validation, supervision, and project administration. A.K.O.: conceptualization, investigation, writing—review and editing, and methodology. R.K.J.: writing—review and editing, methodology, resources, data curation, supervision, formal analysis, software, and project administration. C.T.N.P.: conceptualization, writing—review and editing, methodology, resources, funding acquisition, validation, supervision, and project administration. F.G.: conceptualization, writing—review and editing, methodology, resources, funding acquisition, supervision, and project administration. **Competing interests:** R.T., A.K.O., and F.G. receive support from Agathos Biosciences unrelated to this study. R.K.J. owns stock in Beartooth Biotech and OpenBioWorks, which were not involved in this study. F.G. is a cofounder of Cytex Therapeutics. The other authors declare that they have no competing interests. **Data and materials availability:** All data needed to evaluate the conclusions in the paper are present in the paper and/or the Supplementary Materials. Bulk RNA-seq data are available on GEO (GSE287251), and all other data are available on Dryad (DOI: 10.5061/dryad.dz08kps7c). The FD KO mouse strain can be provided by J.P.A. and X.W. pending scientific review and a completed material transfer agreement. Requests for materials should be sent to J.P.A. (j.p.atkinson@wustl.edu) or X.W. (xwu@wustl.edu).

Submitted 2 October 2024
Accepted 20 March 2025
Published 25 April 2025
10.1126/sciadv.adt5915